Increasing endogenous PPARγ ligands improves insulin sensitivity and protects against diet-induced obesity without side effects of thiazolidinediones

Yu-Hua Tseng (yu-hua.tseng@joslin.harvard.edu)
Joslin Diabetes Center/Harvard Medical School https://orcid.org/0000-0003-2053-9559
Lee-Ming Chuang
National Taiwan University Hospital
Yi-Cheng Chang
National Taiwan University Hospital https://orcid.org/0000-0002-8077-5011
Meng-Lun Hsieh
National Taiwan University Hospital
Lun Tsou
National Health Research Institutes
Shih-Yi Chen
National Taiwan University
Yi-Yu Ke
National Health Research Institutes
Ming-Shiu Hung
National Health Research Institutes
Siow-Wey Hee
National Taiwan University Hospital
Hsiao-Lin Lee
National Taiwan University Hospital
Jiun-Yi Nong
National Taiwan University Hospital
Fu-Hsin Hung
Academia Sinica
Jing-Yong Huang
National Taiwan University Hospital
Fang-Chi Kao
National Taiwan University Hospital
Wei-Shun Yang
National Taiwan University Hospital, Hsin-Chu Branch https://orcid.org/0000-0002-3249-280X
Chu-Hsuan Chiu

National Taiwan University
Shih-Yao Lin
AbGenomics BV, Taiwan Branch
Bi-Yu Liu
University of Kang-Ning
Chi-Ming Tai
E-Da Hospital
Fu-An Li
Institute of Biomedical Sciences, Academia Sinica https://orcid.org/0000-0002-0580-7765
Yet-Ran Chen
Academia Sinica
Ya-Wen Chou
Academia Sinica
Jamie Cheng
Taiwan Liposome Company
Yvonne Shih
Taiwan Liposome Company
Chih-Neng Hsu
National Taiwan University Hospital, Yunlin branch
Juey-Jen Hwang
Cardiovascular center and Division of Cardiology, National Taiwan University Hospital and National Taiwan University College of Medicine
Teng-Kuang Yeh
National Health Research Institutes
Ting-Jen Cheng
Academia Sinica
Tzu-Yu Chen
National Laboratory Animal Center, National Applied Research Laboratories

---

Article

Keywords: type 2 diabetes mellitus, PPARγ, thiazolidinediones

Posted Date: May 14th, 2021

DOI: https://doi.org/10.21203/rs.3.rs-490889/v1

Abstract

Insulin resistance and obesity are pivotal features of type 2 diabetes mellitus. Peroxisome proliferator-activated receptor γ (PPARγ) is a master transcriptional regulator of systemic insulin sensitivity and energy balance. The anti-diabetic drug thiazolidinediones are potent synthetic PPARγ ligands and insulin sensitizers with undesirable side effects including increased adiposity, fluid retention, and osteoporosis, which limit their clinical use. We and others have proved that 15-keto-PGE2 is an endogenous natural PPARγ ligand. 15-keto-PGE2 is catalyzed by prostaglandin reductase 2 (PTGR2) to become inactive metabolites. We found that 15-keto-PGE2 level is increased in Ptgr2 knockout mice. Ptgr2 knockout mice were protected from diet-induced obesity, insulin resistance, and hepatic steatosis without fluid retention nor reduced bone mineral density. Diet-induced obese mice have drastically reduced 15-keto-PGE2 levels compared to lean mice. Administration of 15-keto-PGE2 markedly improved insulin sensitivity and prevented diet-induced obesity in mice. We demonstrated that 15-keto-PGE2 activates PPARγ through covalent binding to its cysteine 285 residue at helix 3, which restrained its binding pocket between helix 3 and β-sheets of the PPARγ ligand binding domain. This binding mode differs from the helix12-dependent binding mode of thiazolidinediones. We further identified a small-molecule PTGR2 inhibitor BPRPT245, which interferes the interaction between the substrate-binding sites of PTGR2 and 15-keto-PGE2. BPRPT245 increased 15-keto-PGE2 concentration, activated PPARγ, and promoted glucose uptake in adipocytes. BPRPT245 also prevented diet-induced obesity, improved insulin sensitivity and glucose tolerance, lowers fasting glucose without fluid retention and osteoporosis. In humans, reduced serum 15-keto-PGE2 levels were observed in patients with type 2 diabetes compared with controls. Furthermore, serum 15-keto-PGE2 levels correlate inversely with insulin resistance and fasting glucose in non-diabetic humans. In conclusion, we identified a new therapeutic approach to improve insulin sensitivity and protect diet-induced obesity through increasing endogenous natural PPARγ ligands without side effects of thiazolidinediones.

Introduction

Insulin resistance is the pathological feature of type 2 diabetes mellitus with obesity as the main contributor. Peroxisome proliferator-activated receptor γ (PPARγ) is a master transcription regulator of insulin sensitivity and systemic energy balance. In the nucleus, PPARγ forms a functional heterodimer with retinoid X receptor (RXR). The PPARγ-RXR complex binds to the PPARγ response elements (PPRE) in the promoter of its target genes. Ligands binding to the ligand-binding domain (LBD) of PPARγ dissociates co-repressors, induces conformational changes of PPARγ, and recruits various transcriptional co-activators to regulate the expression of down-stream genes involved in adipogenesis, glucose and lipid metabolism, thermogenesis, and inflammation (1). Thiazolidinediones (TZDs) are synthetic full PPARγ agonists and potent insulin sensitizers clinically used for treatment of type 2 diabetes. However, TZD use has several undesirable side effects including weight gain, fluid retention, and osteoporosis which limit their clinical application (2). Recent clinical trials of sodium-glucose cotransporter 2 (SGLT2) inhibitors and glucagon-like peptide 1 (GLP-1) analogues have demonstrated that their cardiovascular benefits

derive mainly from weight loss (3,4). Among all current anti-diabetic drugs, only PPARγ agonists and metformin are insulin-sensitizer. Therefore, novel approaches to activate PPARγ without side effects of thiazolidinediones are eagerly awaited and the search for selective or partial agonists devoid of these side effects is actively ongoing (5-9).

We and other groups previously demonstrated that the polyunsaturated fatty acid 15-keto-PGE_2 is a natural endogenous PPARγ ligand derived from PGE_2 that has minimal binding affinity for the prostanoid receptors (10-13). 15-keto-PGE_2 is further catalyzed by prostaglandin reductase 2 (PTGR2) to became inactive metabolite 13,14-dihydro-15-keto-PGE_2 (10). Here, we report that 15-keto-PGE_2 levels are reduced in obese/insulin-resistant mice and human subjects with type 2 diabetes compared with controls. Either genetic or chemical inhibition of PTGR2 or direct administration of 15-keto-PGE_2 improved glucose homeostasis and prevent diet-induced obesity without fluid retention or osteoporosis. We found that the binding mode of 15-keto-PGE_2 PPARγ differs from that of thiazolidinediones. These findings provide a novel avenue for treating diabetes mellitus and obesity without side effects of thiazolidinediones by increasing endogenous PPARγ ligands.

Methods

Generation of *Ptgr2* knockout mice

The generation of *Ptgr2* knockout mice has been described previously (14). Briefly, the mouse *Ptgr2* gene comprises 10 exons with exon 3 containing the catalytic domain. Deletion of exon 3 is predicted to not only delete the catalytic domain but also to create a frameshift mutation resulting in a stop codon in exon 4. The construct used for targeting the *Ptgr2* gene was designed to insert a loxP sequence together with an "FRT-flanked" pgk-neo cassette in intron 2, and a loxP sequence in intron 4. The linearized targeting vector was electroporated into the 129/J embryonic stem cell line and selected by neomycin and ganciclovir. The selected clone was used for blastocyst injection. Immunoblots for Ptgr2 showed deletion of *Ptgr2* in all tissues of knockout mice compared with wild-type controls (**Supplementary Figure 1**).

Animal model

All animal experiments were performed according to institutional ethical guidelines and were approved by the Institutional Animal Care and Use Committee of the Medical College (IACUC) of National Taiwan University. All mice were housed under standard conditions at 23°C and 12/12 hr light/dark (7AM.-7PM.) cycle in animal centers of National Taiwan University Medical College, which is accredited by the Association for Assessment and Accreditation of Laboratory Animal Care International (AAALAC). Mice were fed on either high-fat high-sucrose diet (HFHSD) (cat. no.D12331, Research Diets) or regular chow diet (cat no. 5001, Lab Diet). BPRPT245 was dissolved 3% dimethylacetamide and 10% cremophor in

water and administered to orally HFHSD-fed obese C57BL6/J mice by oral gavage daily (100 mg/kg/day).

Glucose and insulin tolerance test

Glucose tolerance was evaluated by the oral (OGTT) and intraperitoneal glucose tolerance test (ipGTT) after a 6-hr fast. For the OGTT, glucose water (1 mg/g) was given by oral gavage and tail blood glucose was measured with a glucometer (ACCU-CHECK Performa, Roche) at 0, 15, 30, 45, 60, 90, and 120 min. For ipGTT, tail blood glucose was measured at 0, 15, 30, 45, 60, 90, and 120 min after intraperitoneal injection of glucose water (1 mg/g). For the insulin tolerance test (ITT), mice were fasted for 4 hr and then injected intraperitoneally with 1 U/kg of insulin (Humulin R, Eli Lilly). Tail blood glucose was measured at 0, 15, 30, 45, 60, 90, 120, and 180 min.

Measurement of insulin signaling

To evaluate insulin signaling *in vivo*, we fasted the mice overnight. Tissue was harvested 15 min after intraperitoneal insulin injection. The samples (perigonadal fat, inguinal fat, brown adipose tissue and liver) were extracted with RIPA buffer (50 mM Tris-HCl, pH 7.4, 2 mM ethylenediaminetetraacetic acid [EDTA]), 150 mM NaCl, 50 mM NaF, 1% Nonidet P-40, 1 mM phenylmethylsulfonyl fluoride (PMSF), 0.5% sodium deoxycholate, and 0.1% sodium dodecyl sulfate (SDS) containing phosphatase inhibitor cocktail (cat. no. 04693132001, Roche) and homogenized. The homogenates were then centrifuged at 13,000 rpm for 10 min at 4°C to remove debris. Samples were separated by SDS-polyacrylamide gel electrophoresis, transferred to polyvinylidene difluoride (PVDF) membrane, and probed with anti-phospho-Akt antibody (cat. no. 4058, Cell Signaling) and anti-Akt antibody (cat. no. 9272, Cell Signaling) and then with HRP conjugated anti-rabbit IgG antibody (1:10000; cat. no. GTX26721, GeneTex).

Positron emission tomography (PET) / CT (computer tomography) for assessment of glucose uptake

The measurement of glucose uptake in different tissues followed previous protocols (15,16). Briefly, mice were fasted for 4 hrs. A total of 0.5 MBq [^{18}F]-FDG in a 0.1-ml volume was administered through the tail vein and 1.6 U/kg of insulin was injected intraperitoneally immediately following [^{18}F]-FDG administration. Whole body scan was performed for a total of three cycles (10 min per cycle) using PET/CT scanner (eXplore Vista DR, GE). Images were analyzed using the Amide software (17). Region of interest (ROI) was determined using manual selection of sagittal, horizontal, and vertical slices. Standardized uptake values of each ROI (for each tissue) were calculated to estimate glucose uptake.

Formulation for 15-keto-PGE_2 for injection

For animal experiments, 15-keto-PGE_2 was dissolved in liposome (40 mg/kg/day in 20 μL/g/day liposome, intra-peritoneal injection twice daily) for the treatment and was compared to the vehicle-control groups (liposome vehicle 20 μL/g/day, intra-peritoneal injection twice daily) for 3 weeks. The Taiwan Liposome Company designed and provided the liposome formulation.

Preparation of cysteine-coupled 15-keto-PGE_2 and 15-keto-PGF_{2a} proteins

Five mg of ovomucoid (OVO, cat. no. T9253, Sigma-Aldrich) and bovine serum albumin (BSA, cat. no. A2153, Sigma-Aldrich) were dissolved in 1 mL of PBS containing 5% 2-mercaptoethanol and gently agitated at room temperature for 1 hr, respectively. The reduced proteins were buffer-exchanged with PBS using Amicon Ultra-15 Centrifugal Filter Units (cat. no. UFC901024, Millipore) to remove 2-ME. The proteins were then incubated with tenfold molar excess of 15-keto-PGE_2 or 15-keto-$PGF_{2\alpha}$ at room temperature for 1 hr with gentle agitation. The cysteine-coupled proteins, 15-keto-PGE_2-cysteine-OVO, 15-keto-PGE_2-cysteine-BSA, and 15-keto-$PGF_{2\alpha}$-cysteine-BSA, were further buffer-exchanged with PBS to remove free 15-keto-PGE_2 or 15-keto-$PGF_{2\alpha}$ respectively, and stored at 1 mg/mL.

Generation of monoclonal antibodies against cysteine-coupled 15-keto-PGE_2

Ten Balb/c mice (National Laboratory Animal Center, Taiwan) were immunized with 15-keto-PGE_2-cysteine-OVO (100 μg/mouse) emulsified with complete Freund's adjuvant (cat. no. F5881, Sigma-Aldrich) via subcutaneous injection. After four weeks, mice were subcutaneously injected with 15-keto-PGE_2-cysteine-OVO (100 μg/mouse) emulsified with incomplete Freund's adjuvants (cat. no. F5506, Sigma-Aldrich) three times at a two-week intervals. Mice received 10 μg of 15-keto-PGE_2-cysteine-OVO via tail vein three days prior to spleen harvest. Hybridomas were prepared by fusing spleen cells with the mouse myeloma cell line FO (cat. no. CRL-1646, ATCC) using PEG 1500 (cat. no. 10783641001, Roche). The fusion procedures followed the manufacturer's manual. Hybridomas were selected in complete Dulbecco's modified Eagle's medium (DMEM) containing hypoxanthine-aminopterin-thymidine (cat. no. 11067030, Thermo Fisher) and UltraCruz Hybridoma Cloning Supplement (cat. no. sc-224479, Santa Cruz) for 12-14 days. Cell culture supernatants were screened with ELISA using 15-keto-PGE_2-cysteine-BSA as antigens. Positive hybridomas were then cloned by limiting dilution. Antibody isotypes were determined with a Rapid ELISA Mouse mAb Isotyping Kit (cat. no. 37503, Thermo Fisher). Monoclonal antibodies were purified from hybridoma culture supernatants using Protein A Sepharose CL-4B (cat. no. 17078001, GE). The purification procedures were performed according to the manufacturer's manual. Four anti-cysteine-coupled 15-keto-PGE_2 hybridoma clones were prepared. Clones 1A6 and 17E7 had superior specificity and reacted only to cysteine-coupled 15-keto-PGE_2 (**Supplementary Figure 2**).

Cell culture

All cells were cultured at 37°C, 5% CO_2 in a humidified incubator. HEK293T cells were maintained in DMEM (cat. no. SH30003.02, HyClone) supplemented with 10% fetal bovine serum (FBS) (cat. no. 04-001-1A, Biological Industries) and 1% antibiotic/antimycotic solution (cat. no. SV30079.01, HyClone). 3T3-L1 preadipocytes were maintained at ~70 % confluence in DMEM with 10% calf serum (cat. no. 16170078, Gibco) and 1% antibiotic/antimycotic solution. For adipocyte differentiation, confluent 3T3-L1 cells (defined as day 0) were exposed to induction medium containing 10% FBS, 1 μM dexamethasone (cat. no. D4902, Sigma-Aldrich), and 1 μg/ml insulin (Humulin R, Eli Lilly) in DMEM with or without 0.5 mM isobutyl-methylxanthine (cat. no. sc-201188A, Santa Cruz Biotechnology) as indicated. After two days, the medium was replaced with DMEM containing 10% FBS and 1 μg/ml insulin, and was replenished every two days until assay.

RNA extraction, cDNA synthesis and real-time quantitative PCR (RT-qPCR)

A total of 1×10^5 of 3T3-L1 preadipocytes were seeded in 6-well plates, and differentiated for six days, then the 3T3-L1 adipocytes were harvested in 1 ml of REzol C&T (cat. no. PT-KP200CT, Protech), and total RNA was extracted according to the manufacturer's instructions with slight modifications. Briefly, 200 μl of chloroform was added to 1 ml of sample in REzol, and samples were mixed vigorously by shaking for 30 sec, followed by incubation at room temperature for 5 min. Then, samples were centrifuged at 12,000 g for 15 min at 4°C, and 400 μl of the upper aqueous phase were transferred to a new 1.5-ml tube. An equal volume of isopropanol was added. Samples were inverted several times for mixing and then centrifuged at 12,000g for 10 min at 4°C. The RNA precipitate, which formed a pellet at the bottom of 1.5-ml tube, was washed for three times with 75% ethanol and air-dried for 15 min. Pellets were dissolved the in RNase-free water. The concentration of RNA was measured using Nanodrop. cDNA was synthesized using a reverse transcription kit (cat. no. K1622, Thermo Scientific) using the oligo(dT)18 primers. RT-qPCR was performed in a 10-μl reaction with 50 ng cDNA and 0.4 M primer using SYBR green reagent (cat. no. 11203ES08, YEASEN). Mouse peptidylprolyl isomerase A (*Ppia*) mRNA was used as the internal control. RT-qPCR reactions were performed using ABI 7900HT FAST (Applied Biosystems) and Sequence Detection Systems (SDS v2.3, Applied Biosystems). All qPCR reactions were run in duplicates. The primers used are listed in **Supplementary Table 1.**

Plasmid construction and site-directed mutagenesis

Murine PPARγ plasmid (pCMV6-Pparg) was purchased from OriGene (cat. no. MC201042, OriGene, USA). A cysteine-313 to alanine (C313A) substitution of mPPARγ construct was generated with the

mutagenesis kit (cat. no. 210518, Agilent, USA) following the standard manufacturer's protocol. Primers site-directed mutagenesis was designed using a web-based program (http://www.genomics.agilent.com/primerDesignProgram.jsp) (**Supplementary Table 2).**

Reporter assay

Gal4-PPARγ/UAS-LUC reporter assay was conducted as previously described (12) with minor modifications. Briefly, HEK293T cells were seeded at 1×10^5 cells/well in 24-well plates. After 24- hrs growth, a DNA solution containing UASG reporter construct, GAL4-PPAR expression vector and TK-Rluc (Renilla luciferase) reporter construct (internal control) was transfected using TurboFect™ transfection reagent (cat. no. R0532, Thermo Fisher). Cells were treated and harvested after another 24 and 48 hrs, respectively. The luciferase activity was measured by Luc-Pair™ Duo-Luciferase HS Assay Kit (cat. no. LF600, Promega) and normalized to the TK reporter signal. For the PPRE reporter assay, as described above, 24 hrs after seeding HEK293T cells, PPRE-LUC reporter vector, TK-Rluc reporter and wild-type or mPPARγ C313A were transfected into cells using TurboFect transfection reagent.

Insulin-stimulated glucose uptake assay

Differentiated 3T3-L1 cells were starved with serum-free DMEM containing 0.2% BSA (cat. no. A9647, Sigma-Aldrich). Cells were rinsed twice with KRH buffer (137 mM NaCl, 4.7 mM KCl, 1.85 mM CaCl2, 1.3 mM MgSO4, 50 mM HEPES and 0.1% BSA, pH 7.4), and treated with or without 1 µg/mg insulin in the presence of 20 µM cytochalasin B (cat. no.11328, Cayman Chemical), a GLUT inhibitor for measuring non-specific glucose uptake, for 30 min. Cells were then incubated with 0.5 µCi [^{3}H]-2-deoxy-D-Glucose (cat. no. NET328A001MC, PerkinElmer) and 0.1 µM 2-deoxy-D-Glucose (2DG) (cat. no. 14325, Cayman Chemical) for 5 min. Uptake of 2DG was terminated by a rapid removal of medium and washing with ice-cold PBS three times. Cells were lysed with 0.1% SDS, and the radioactivity was measured using a liquid scintillation counter. Insulin-mediated glucose uptake was calculated by subtracting insulin-treated glucose uptake with basal glucose uptake (in absence of insulin).

Computer modeling analysis binding between PPARγ and 15-keto-PGE_2

Docking analyses were conducted using the CovalentDock program (18). The human X-ray structure of PPARγ (PDB ID: 5Y2O) (19) was used to assess for covalent binding with the small molecule 15-keto-PGE_2. To illustrate the binding mode of 15-keto-PGE_2, the covalent docking approach was applied. To ensure mimicking the experiment results of mouse species, four amino acids (S302N, V307I, L435V, and Q454H) were mutated by computer modeling. To bring the docked ligand-protein complex to equilibrium, molecular dynamics simulations were performed using the BIOVIA 2017/Standard dynamics Cascade

program (BIOVIA, Inc., San Diego, CA). The minimization convergent was used in two steps, namely, Steepest Descent with RMS gradient convergent to 1, and the final step of Adopted Basis NR with RMS Gradient convergent to 0.1. The default parameters were used for the simulation, except for the Production parameter, which was set as 20 ns. All the minimization process was performed in an aqueous environment following the Distance-Dependent Dielectrics methods. After the molecular dynamics simulation, the binding energy of these two molecules was calculated using the BIOVIA 2017/Calculate Binding Energies program (BIOVIA, Inc., San Diego, CA). Three-dimensional models were displayed by using the PyMOL program (20).

To evaluate the interaction between PTGR2 inhibitor BPRPT245, 15-keto-PGE_2, NADPH, and PTGR2, the X-ray structure of human PTGR2 (PDB ID: 2ZB4) was used. Ligand energy was minimized using PyRx program before docking (21). The 2D protein-ligand interaction diagrams are presented by using the LigPlot+ program (22).

Immunoprecipitation and proteomic analysis

For immunoprecipitation, HEK293T cells were transfected with mouse PPARγ (mPPARγ) and mPPARγ C313A plasmids, which are Myc-DDK-tagged (OriGene, USA). After 24 hr, cells were treated with dimethyl sulfoxide (DMSO) or 30 μM 15-keto-PGE2 for an additional 24 hrs and harvested with cell lysis buffer (50 mM Tris HCl, pH7.4, 1 mM EDTA, 150 mM NaCl, and 1% Triton X-100). Proteins were immunoprecipitated using Anti-FLAG® M2 Magnetic Beads (cat. no. F1804, Sigma-Aldrich) according to the manufacturer's protocol. Subsequently, the eluted proteins were separated by SDS-PAGE and subjected to immunoblot analysis. Following separation by SDS-PAGE, proteins were stained with Coomassie blue and SYPRO-Ruby stain. The protein bands of interest were cut out for in-gel tryptic digestion followed by C18 Zip-Tip clean-up (Millipore, USA). For shotgun proteomic identifications, nanoLC-nanoESI-MS/MS analysis was performed on a nanoAcquity system (Waters, USA) connected to the LTQ Orbitrap Velos hybrid MS (Thermo Electron, USA) equipped with a PicoView nanospray interface (New Objective, USA). Samples were loaded onto a C18 BEH column (75 μm × 25 cm length, 130 Å , 1.7 μm particle size) (Waters, USA) and separated by a segmented gradient form in 60 min from 5% to 40% acetonitrile (with 0.1% formic acid) at a constant flow rate of 300 nL/min with a column temperature of 35°C. The mass spectrometer was operated in the data-dependent mode. Full scan MS spectra were acquired in the Orbitrap at 60,000 resolution (at m/z 400) with automatic gain control target of $5´10^5$. The 10 most abundant ions were isolated for high-energy collision dissociation, MS/MS fragmentation and detection in the Orbitrap. For MS/MS measurements, a resolution of 7500, an isolation window of 2 m/z and a target value of 50,000 ions, with maximum accumulation times of 100 ms were used. Fragmentation was performed at 35% normalized collision energy and an activation time of 0.1 ms. Ions with single and unrecognized charge state were excluded. Protein identification and modification were analyzed using Mascot Daemon (Matrix Science Inc.).

Generation of PPARγ-null 3T3-L1 stable cell lines using CRISPR/Cas9 System

Gene editing was performed in 3T3-L1 preadipocytes using the clustered regularly interspaced short palindromic repeats (CRISPR)/Cas 9 system. Two single-guide RNAs (sgRNA) (**Supplementary Table 3**) targeting exon 6 of mouse *Pparg* were designed using a web-based design tool (http://crispr.mit.edu/). These oligonucleotides were cloned into the pSurrogate reporter and pAll-Cas9.Ppuro vector obtained from Academia Sinica, Taiwan. The pSurrogate reporter contains an EGFP and an out-of-frame mCherry located downstream of the sgRNA; the pAll-Cas9.Ppuro vector expresses Cas9 nuclease and sgRNA. Once a double-stand break at target site in pSurrogate reporter plasmid was created by Cas9, insertions and deletions (indels) could be introduced at the cleaved site. The indels cause frameshifts and resulted in expression of the mCherry gene. 3T3-L1 preadipocytes were co-transfected with pSurrogate reporter and pAll-Cas9.Ppuro vector at 80-90% confluency using PolyJet™ transfection reagent (cat. no. SL100688, SignaGen Laboratories, USA). Two days after transfection, EGFP/mCherry double-positive cells were enriched by fluorescent-activated cell sorting. Single cells were isolated and expanded. The genomic DNA was amplified by PCR and sequenced to confirm the knockout cell lines. The primer sequences are shown in the **Supplementary Table 3**.

Lentivirus production and transduction

The mPPARγ C313A cDNA sequence was amplified from pCMV6-Pparg C313A and

subcloned into the XhoI/NotI restriction sites of the pLVX-IRES-Neo vector. The lentiviral expression plasmids, pMD.G and pCMVΔR8.91 (RNAi Core, Academia Sinica, Taiwan) were co-transfected into HEK293T cells. The medium containing lentivirus was collected at 40 and 64 hr after transfection, and centrifuged at 1,200 rpm for 5 min and then filtered through a 0.45-μm filter. PPARγ-null 3T3-L1 preadipocytes were infected with the lentivirus in the presence of 10 μg/ml polybrene (cat. no. sc-134220, Santa Cruz). Then, 48 hrs after infection, the cells were selected with 400 μg/ml G418. The expression of PPARγ was verified by immunoblotting using anti-PPARγ antibody (cat. no. sc-7273, Santa Cruz). HSP70 was probed with anti-HSP70 antibody (cat. no. ab45133, Abcam) as a loading control.

15-keto-PGE_2 extraction from tissues and cultured cells

Tissue was homogenized in liquid nitrogen using pestle and mortar. Approximately 500 mg of tissue homogenate was treated with 400 μL of the upper layer of acetonitrile/hexane mixture supplemented with 2 μL formic acid. The homogenate was then added with 600 μL acetonitrile containing 13,14 dihydro-15-keto-PGE_2-d4 (cat no. 10007978, Cayman Chemical, Ann Arbor, MI) in 1:20,000 dilution, followed by addition of 600 μL ddH_2O. The mixture was centrifuged at 12,000 rpm for 10 min at 0°C. The

lower layer was then transferred to a new tube. A C-18 solid-phase extraction (SPE) cartridge (Cat no. 400020, Cayman Chemical) was first activated with 20 mL methanol and then with 20 mL ddH_2O. The SPE cartridge was subsequently washed with 5 mL 15% methanol and then with 5 mL ddH_2O. The sample was then eluted with 10 mL HPLC-degree methanol (Methanol Chromasolv LC-MS, Fluka) into a new 2-mL tube and was then air-dried by the SpeedVac system (Savant SPD1010, Thermo Scientific). The dried samples were stored in -80°C. The samples were reconstituted with 100 µL methanol before LC-MS/MS.

For 15-keto-PGE_2 extraction from cultured cells (in 6-well culture plates), the medium was removed and cells were scraped by adding 500 µL methanol containing 13,14 dihydro-15-keto-PGE_2-d4 (1:20000 dilution), followed by addition of 1 mL PBS buffer. The homogenate was centrifuged at 300g for 5 min to remove cellular debris. The supernatant was transferred to a new tube. The C-18 SPE cartridge was first activated with 2 mL methanol and then 2 mL ddH_2O. The lower-layer sample was transferred to C-18 SPE cartridge. The SPE cartridge was subsequently washed with 2 mL 15% methanol and 5 mL ddH_2O. The sample was then eluted with 5 mL HPLC-degree methanol into a new 2-mL tube and air-dried using a SpeedVac system. The dried samples were stored in -80°C. The dried samples were reconstituted with 60 µL methanol before analysis.

Human subjects for measurement of serum 15-keto-PGE_2 levels

Fifty non-diabetic male participants were recruited from a community-based screening for diabetes mellitus in the Yunlin County in Taiwan. We recruited another 24 male patients with type 2 diabetes from the metabolic clinic of Yunlin branch of National Taiwan University Hospital and selected 24 age- and body mass index (BMI)-matched male non-diabetic patients from a community-based screening program. The study protocol was approved by the Institutional Review Board of the National Taiwan University Hospital. Written informed consent was obtained from every participating subject. All procedures performed in studies involving human participants were in accordance with the Declaration of Helsinki.

Measurement of 15-keto-PGE_2 by liquid chromatography-tandem mass spectrometry analysis (LC-MS/MS)

LC-MS/MS quantification methods were performed as described previously (14). In the LC-MS/MS analysis, an ultra-high performance liquid chromatography (UHPLC) system (ACQUITY UPLC, Waters, Milford, MA) was coupled to a linear ion trap-orbitrap mass spectrometer (Orbitrap Elite, Thermo Scientific). Solvent A of 2% acetonitrile and 0.1% formic acid in deionized water and solvent B of 0.1% formic acid in acetonitrile were used as the mobile phase for UHPLC separation. The metabolites were separated with a reverse phase column (HSS T3, 1.8 µm, 2.1 mm×100 mm, Waters, Milford, MA) at the flow rate of 500 µL/min using gradients of 40% solvent B at 0–1 min, 40–50% solvent B at 1–3 min, 50–

80% solvent B at 3–6 min, 80–99.5% solvent B at 6–8 min, 99.5–99.5% solvent B at 8–9 min, 99.5–40% solvent B at 9–9.01 min and 40–40% solvent B at 9.01–10 min. The total chromatography separation time for each analysis was 10 min and the column temperature was set to 40 °C. The mass spectrometer was operated in the ESI negative-ion mode with an electrospray voltage of 2.5 kV, capillary temperature 360 °C and source heater temperature 350 °C. Mass spectra were acquired by cycling a full MS scan with a range of mass-to-charge ratios (*m/z*) of 275-360 and two product ion scans for 13,14-dihydro-15-keto-PGE_2 (*m/z* 351.21) and 15-keto-PGE_2 (*m/z* 349.2). The fragmentation reactions of *m/z* 351.21 to 333.207 and *m/z* 349.2 to 331.191 were selected for the quantitation of 13,14-dihydro-15-keto-PGE_2 and 15-keto-PGE_2. All data were acquired and processed using Xcalibur software (Thermo Scientific)

High-throughput compound screening (HTS)

High-throughput compound screening was conducted at the core service in Genomics Research Center (GRC) of Academia Sinica, Taiwan. The GRC 120K ReSet comprises more than 125,000 compounds, which were selected as representatives by structural similarity clustered from the 2M GRC compound library. The ReSet was arrayed in 1,536-well plates as single compounds at 1 mM in 100% DMSO. The quality of all compounds was assured by the vendor (purity is greater than 90%) and was verified internally with 5% random sampling. Recombinant human PTGR2 protein was purified and the screening was conducted using the NADPH-Glo Detection kit (Promega) to measure the amount of NADPH. The CV of HTS ranged from 4.8 % to 6.1 % with a Z' value of 0.7. The threshold was set to 1.5, resulting ~300 hits for further confirmation and determination of the half-maximal inhibitory concentration (IC50). Eight-point two-fold dilution of the compounds were prepared for IC50 determination and used in dose-dependent studies. The compounds showing dose-dependent increases of unused NADPH indicated the activities of recombinant human PTGR2 enzymatic activity.

Measurement of bone mineral density

The bone mineral density of cortical bone of femur were quantified and imaged using a benchtop Micro-CT imager (SkyScan 1076 in vivo, Bruker-MicroCT, Belgium) at 35 μm voxel image resolution with voltage of 50 kV, current of 200 μA, and exposure time of 140 ms, using a 0.5 mm aluminum filter.

Cold-induced and diet-induced thermogenesis

For the cold tolerance test, 24-week-old mice with matched average body weight from the two groups were placed individually on HFHSD in a 4°C chamber. The rectal temperature of the mice was measured after 0, 1, 2, 3, 4, 5, 6, 12, and 18 hours. For the diet-induced thermogenesis test, 24-week-old mice were

fasted overnight for 18 hours. Then, their rectal temperature was measured at 0, 30, 60, 90, 120, 150, 180, and 240 min after HFHSD refeeding.

Statistical analysis

All values were expressed as mean ± S.E.M. All reported sample sizes were biologically independent values but not technically repeatedly measured values. Comparisons between two independent groups were performed using Student t-tests. Comparisons between multiple groups were conducted using one-way analysis of variance with post hoc analyses. Two-sided P-values < 0.05 were considered as statistically significant. Statistical analyses were conducted using GraphPad Prism 8.0 and SAS 9.0.

Results

Ptgr2 knockout mice with increased 15-keto-PGE_2 exhibited less diet-induced weight gain and improved insulin sensitivity without fluid retention and osteoporosis

Several studies have proved 15-keto-PGE_2 as a natural endogenous PPARγ ligand derived from PGE_2 (10-13). 15-keto-PGE_2 can be irreversibly metabolized by prostaglandin reductase 2 (PTGR2) into the inactive metabolite 13,14-dihydro-15-keto-PGE_2 (**Figure 1a**). To investigate the effects of increasing 15-keto-PGE_2 on systemic glucose homeostasis and energy metabolism, we generated *Ptgr2* knockout mice (*Ptgr2*$^{-/-}$) which lack the inactivating enzyme of 15-keto-PGE_2. As expected, *Ptgr2* expression was abolished in all tissues of *Ptgr2*$^{-/-}$ mice (**Supplementary Figure 1**). The concentrations of 15-keto-PGE_2 increased significantly in serum (**Figure 1b**) and white fat (**Figure 1c**) and of *Ptgr2*$^{-/-}$ mice.

When fed with regular chow, there was no differences in body weight, fasting glucose, glucose tolerance, and insulin sensitivity between knockout mice and controls (**Supplementary Figure 3**). However, upon high-fat high-sucrose feeding (HFHSD) feeding, *Ptgr2*$^{-/-}$ mice exhibited significantly less body weight gain (**Figure 1d**) and lower fasting glucose levels as compared with wild-type littermates (*Ptgr2*$^{+/+}$) (**Figure 1e**). *Ptgr2*$^{-/-}$ mice were more glucose-tolerant (**Figure 1f**) and more insulin-sensitive (**Figure 1g**) than controls. ^{18}F-FDG -positron emission tomography (PET) showed higher ^{18}F-FDG uptake following insulin stimulation in the perigonadal fat and inguinal fat tissue of *Ptgr2*$^{-/-}$ mice compared with controls (**Figure 1h, 1i**). Consistently, the immunoblots showed significantly increased phospho-Akt levels in perigonadal fat, inguinal fat, and liver but not in skeletal muscle of *Ptgr2*$^{-/-}$ mice after insulin injection (**Figure 1j**). There is a also a trend of increased phospho-Akt levels in the brown adipose tissue (BAT) of *Ptgr2*$^{-/-}$ as compared to wild-type controls.

The inguinal fat, brown fat, and liver of *Ptgr2*$^{-/-}$ mice were smaller than controls under HFHSD (**Figure 1k**). Body composition analysis revealed significantly lower fat content in *Ptgr2*$^{-/-}$ mice than in controls, while lean mass was not altered (**Figure 1l**). Importantly, the free fluid (water contained in urine), total water

(water contained in urine, tissue and blood) (**Figure 1l)**, and mineral density of the femur of *Ptgr2*$^{-/-}$ mice were similar to those observed in controls (**Figure 1m, 1n**). The adipocyte size was smaller and the adipocyte number was not significantly reduced in the perigonadal fat of *Ptgr2*$^{-/-}$ mice (**Figure 1o, 1p**). Immunohistochemical staining showed fewer F4/80-positive infiltrating macrophages and crown-like structure in the perigonadal fat of *Ptgr2*$^{-/-}$ mice compared with the control animals (**Figure 1q, 1r**).

The H&E stain of the liver showed lesser degree of hepatic steatosis (**Figure 1s**) and the hepatic triglyceride content is lower in *Ptgr2*$^{-/-}$ mice than controls (**Figure 1t**). Fasting serum levels of total cholesterol, leptin, and insulin were also lower in *Ptgr2*$^{-/-}$ mice (**Supplementary Figure 4**).

To explore the mechanism by which *Ptgr2*$^{-/-}$ mice are leaner than wild-type controls, we examined their energy balance. Indirect calorimetry performed at the age of 8 weeks, when the body weight were not different between two groups, showed significantly higher oxygen consumption (VO_2) (**Figure 2a**) and energy expenditure (**Figure 2b**) during dark phase (active phase) in *Ptgr2*$^{-/-}$ mice than in controls. There were no differences in food intake (**Figure 2c**), physical activity (**Figure 2d**), or fecal triglyceride content (**Figure 2e**) between knockout and wild-type mice. Grossly, the inguinal fat, perigonadal fat, and brown adipose tissue of *Ptgr2*$^{-/-}$ mice were browner in appearance (**Supplementary Figure 5**). Immunoblots showed increased *Ucp1* protein expression in all fat depots of *Ptgr2*$^{-/-}$ mice compared with controls (**Figure 2f**). RT-qPCR showed higher expression of genes involved in browning, including *Ucp1, Dio2,* and *Cidea* in brown fat, inguinal fat, and perigonadal fat of *Ptgr2*$^{-/-}$ mice (**Figure, 2g, 2h, 2i**).

Furthermore, we evaluated diet- and cold-induced thermogenesis in *Ptgr2*$^{-/-}$ mice and controls. We found a significantly increased body surface temperature in the interscapular and inguinal regions, and core rectal temperature after HFHSD feeding (**Figure 2j, 2k, 2l**) in *Ptgr2*$^{-/-}$ mice. Similarly, *Ptgr2*$^{-/-}$ mice displayed higher surface interscapular, surface inguinal, and core rectal temperature when exposed to cold environment (**Figure 2m, 2n, 2o**). These data showed enhanced thermogenesis in *Ptgr2*$^{-/-}$ mice, probably due to browning of fat tissues.

15-keto-PGE_2 increases insulin-stimulated glucose uptake and activates PPARγ through binding to the cysteine residue of PPARγ

To investigate the mechanism by which *Ptgr2*$^{-/-}$ mice showed improved insulin sensitivity and increased glucose uptake, primary white preadipocytes were isolated from *Ptgr2*$^{-/-}$ mice and then induced into mature adipocytes. We found that primary adipocytes isolated from the stromal vascular fraction (SVF) of the inguinal fat of *Ptgr2*$^{-/-}$ mice displayed increased insulin-stimulated glucose uptake compared with wild-type controls (**Figure 3a**). In view of the increased 15-keto-PGE_2 levels in *Ptgr2*$^{-/-}$ mice, we treated induced 3T3-L1 adipocytes with 15-keto-PGE_2 and found that 15-keto-PGE_2 increased insulin-stimulated glucose uptake in a dose-dependent manner. The effect of 10 μM 15-keto-PGE_2 was similar to that of 1

μM pioglitazone, while 13,14-dihydro-15-keto-PGE_2 has little effect (**Figure 3b**). Of note, the maximal dose of exogenously added 15-keto-PGE_2 (10-20 μM) resulted in an approximately 1.5-3 fold increase of the physiological intracellular 15-keto-PGE_2 levels, suggesting near-physiological intracellular 15-keto-PGE_2 levels are sufficient to increase insulin-stimulated glucose uptake (**Supplementary Figure 6**).

Using the Gal4-PPARγ/UAS-LUC reporter assay system, we found that 15-keto-PGE_2 dose-dependently enhanced the transactivation activity of PPARγ (**Figure 3c**). Expression of *Glut4* (**Figure 3d**) and other PPARγ downstream genes involved in insulin signaling (*Irs2*, *Sorbs1*) (**Figure 3e, 3f**), lipid metabolism (*Cd36, Acs)* (**Figure 3g, 3h**), and adipogenesis *(Cebpa, Adipq*) (**Figure 3i, 3j**) were significantly increased in 15-keto-PGE_2-treated 3T3-L1 adipocytes.

To explore how 15-keto-PGE_2 activated PPARγ, murine PPARγ2 (Myc-DDK tagged) was over-expressed in HEK293T cells, which were then incubated with 15-keto-PGE_2. Cell lysates were then separated by SDS-PAGE and stained with Coomassie blue. The protein band around 60 kDa was excised from the gel, and was digested in-gel. The peptides were further analyzed by LC-MS/MS. The results showed that 15-keto-PGE2 was covalently coupled to mPPARγ2 at cysteine 313 residue (C313) (**Figure 3k**). To confirm the data obtained from LC-MS/MS, we performed reciprocal immunoprecipitations to confirm the interaction between 15-keto-PGE_2 and murine PPARγ2. We generated a monoclonal antibody against 15-keto-PGE_2 conjugated to the cysteine residues of BSA. HEK293T cells were transfected with Myc-DDK-tagged murine PPARγ and treated with 15-keto-PGE_2. Cell lysates were first immunoprecipitated with anti-FLAG antibody and then immunoblotted with monoclonal anti-15-keto-PGE_2-cysteine-BSA antibody. A single band of PPARγ (57 kDa) was detected in samples expressing wild-type murine PPARγ but not in samples expressing mPPARγ with C313A mutation (**Figure 3l)**. Reciprocally, when protein lysates were immunoprecipitated with anti-15-keto-PGE_2-cysteine-BSA antibody and then immunoblotted with anti-FLAG antibody, a band of approximately 57 kDa was detected only in cells over-expressing wild-type mPPARγ but not mPPARγ with C313A mutation (**Figure 3l)**. These data revealed the critical role of C313 residue of PPARg in facilitating the covalent binding of 15-keto-PGE_2. The reciprocal co-immunoprecipitation experiments confirmed that 15-keto-PGE_2 binds to mPPARγ at Cys313 residue (**Figure 3m**).

We then expressed wild-type mPPARγ or mPPARγ with the C313A mutation in HEK 293T cells transfected with PPARγ transactivation reporter (PPRE). The addition of 15-keto-PGE_2 dose-dependently increase the reporter activity of PPARγ, which was abolished in cells expressing mutant mPPARγ (C313A), suggesting that 15-keto-PGE_2 activates PPARγ through cysteine 313 residue (**Figure 3n)**. To further confirm the role of mPPARγ Cys313 in 15-keto-PGE_2-induced glucose uptake of cultured adipocytes, insulin-stimulated glucose uptake assay was conducted in PPARγ-null 3T3-L1 cells expressing either wild-type or C313A mutant mPPARγ. PPARγ-null 3T3-L1 cells were generated by CRISPR/Cas9 genome editing technique. Two PPARγ-null 3T3-L1 clones were tested: #1296 was generated using sgRNA#1 and #2328 was generated using sgRNA#2 (**Supplementary Figure 7a, 7b**). Wild-type and C313A mutant mPPARγ were introduced to PPARγ-null 3T3-L1 clones, which were then induced to mature adipocytes. We found that

15-keto-PGE_2 enhanced insulin-stimulated glucose uptake in clone # 1296 rescued with wild-type mPPARγ (**Figure 3o)** but not in the same clone rescued with mutant mPPARγ (C313A) (**Figure 3p, Supplementary Figure 7a, 7b).** Similar findings were also observed in #2328 clones rescued with wild-type and C313A mutant mPPARγ (**Supplementary Figure 7c, 7d**). These results clearly confirmed that Cys313 of mPPARγ is required for 15-keto-PGE_2-induced enhanced insulin-stimulated glucose uptake response.

As *Ptgr2* knockout mice develop browning of fat tissues, cultured 3T3-L1 cells were employed to explore whether browning is mediated through prolonged treatment with 15-keto-PGE_2. We found that 3 weeks of treatment with 15-keto-PGE_2 or pioglitazone but not 13,14-dihydro-15-keto-PGE_2, significantly increased *Ucp1* protein levels in differentiated 3T3-L1 adipocytes in a concentration-dependent manner (**Figure 3q**).

The binding pocket of 15-keto-PGE_2 to PPARγ is different from pioglitazone

Molecular docking showed that the binding site of 15-keto-PGE_2 to the human PPARγ (hPPARγ) LBD differs from that of pioglitazone. Consistent with previous analyses (19, 23), pioglitazone forms hydrogen bond with Tyr473 (helix 12), His449 (helix 11), His323 (helix 5), and Ser289 (helix 3) residues of hPPARγ LBD with a binding energy of -43.37 Kcal/mol **(Figure 4a)**. The thiazolidine-2,4-dione group of pioglitazone formed strong hydrogen bonds with Tyr473 at helix 12, thereby stabilizing helix 12 **(Figure 4b)**. In contrast, 15-keto-PGE2 formed a covalent bond with Cys285 of hPPARγ at helix 3 with a binding energy of -74.15 Kcal/mol which is lower than that of pioglitazone **(Figure 4c)**. The Cys285 residue of hPPARγ is equivalent to Cys313 residue of mPPARγ. 15-keto-PGE2 also forms hydrogen bond with Tyr327 (helix 5), Arg288 (helix 3), and Ile326 (helix 5). The strong covalent bond between 15-keto-PGE2 with Cys285 at helix 3 restrain 15-keto-PGE2 within the binding pocket between helix 3, helix 5, and the β sheets, distant from helix 12 (**Figure 4d)**. The binding pattern is very similar to selective or partial PPARγ agonist MRL24 or SR1664, which is demonstrated to activate PPARγ through helix-12 independent mechanism (**Supplementary Figure 8)**.

15-keto-PGE_2 levels are decreased in patients with type 2 diabetes and insulin-resistant/obese mice and 15-keto-PGE_2 treatment protected against diet-induced obesity and improved insulin resistance without fluid retention and osteoporosis

In humans, the serum level of 15-keto-PGE_2 was significantly reduced in 24 individuals with type 2 diabetes compared with 24 age- and sex-matched non-diabetic controls (175.5±14.15 vs 366.9±27.34 pM) (**Figure 5a)**. In 50 non-diabetic humans, serum level of 15-keto-PGE_2 was inversely correlated with Homeostasis Model Assessment of Insulin resistance (HOMA-IR) (r=-0.37, P=0.007), fasting glucose (r=-0.31, P= 0.02), and fasting insulin (r=-0.33, P= 0.02) (**Figure 5b, 5c, 5d**), but not with BMI (**Figure 5e)**. These findings evidenced the association of endogenous PPARγ ligand 15-keto-PGE_2 levels with insulin sensitivity and glucose homeostasis in humans.

Previous reports showed that during 3T3-L1 adipocyte differentiation, *Ptgr2* expression increases while 15-keto-PGE_2 level decreases progressively (10, 24). We also found that *Ptgr2* is enriched in mature adipocytes but not in the SVF isolated from white and brown fats of C57BL6/J mice (**Supplementary Figure 9**). Consistently, serum levels of 15-keto-PGE_2 were markedly reduced in HFHSD-induced obese mice compared with chow-fed lean mice (**Figure 5f)**. 15-keto-PGE_2 content in perigonadal fat (**Figure 5g)** and inguinal fat (**Figure 5h)** were similarly reduced in HFHSD-induced obese mice compared with controls.

In view of the low 15-keto-PGE_2 levels observed in obese mice, we sought to examine whether 15-keto-PGE_2 can rescue obesity and insulin resistance in mice. We administered 15-keto-PGE_2 in HFHSD-fed obese C57BL6/J mice for 3 weeks. 15-keto-PGE_2 protected against diet-induced obesity (**Figure 5i)** and markedly improved glucose tolerance (**Figure 5j)** and insulin sensitivity (**Figure 5k)** in HFHSD-fed mice. Immunoblots showed increased phospho-Akt in perigonadal fat, inguinal fat, brown adipose tissue, and liver (**Figure 5l)** of 15-keto-PGE_2-treated mice. White fat mass was also reduced in mice treated with 15-keto-PGE_2 (**Figure 5m)** and body composition analysis showed reduced fat mass without fluid retention (**Figure 5n)**. Moreover, the adipocyte size was smaller (**Figure 5o, 5p)** in 15-keto-PGE_2-treated mice but there was no significant difference in adipocyte number (**Figure 5q)**. Higher energy expenditure (**Figure 5r)** was observed in mice treated with 15-keto-PGE_2 as compared to vehicle controls when there was no difference in body weight between the two groups at age of 8 weeks. Food intake (**Figure 5s)** and physical activity (**Figure 5t)** were similar between mice treated with 15-keto-PGE_2 and vehicle. Similar to *Ptgr2*$^{-/-}$ mice, mice receiving 15-keto-PGE_2 had increased expression of *Ucp1* in inguinal, perigonadal, and brown adipose tissues (**Figure 5u**). Similarly, mice receiving 15-keto-PGE_2 exhibited higher interscapular, inguinal, and rectal temperature after HFHSD feeding (**Figure 5v).** Furthermore, mice receiving 15-keto-PGE_2 exhibited higher interscapular, inguinal, and rectal temperature than vehicle controls during prolonged cold tests (**Figure 5w)**, indicating that 15-keto-PGE_2 increases diet and cold-induced thermogenesis.

A PTGR2 chemical inhibitor prevents diet-induced obesity and improves insulin resistance and glucose intolerance via activating PPARγ

Based on these exciting data from the *Ptgr2*$^{-/-}$ mice, we next searched for druggable chemical inhibitors that can effectively suppress PTGR2 enzymatic activity. Using a high-throughput screen of 12,500 chemicals, we identified 31 hits and generated 262 derivatives based on a molecular hybridization strategy between the hits. The *in vitro* IC50 (the half- maximal inhibitory concentration) was evaluated and the compound's activity to restore 15-keto-PGE_2-dependent PPARγ trans-activation in HEK293T cells expressing recombinant PTGR2. EC50 (the concentration for half-maximal effect) was also profiled. Of the 262 newly synthesized inhibitors, a derivative of triazole-pyrimidione (BPRPT245) (**Figure 6a**) exhibited an IC50 of 8.92 nM and an EC50 of 49.22 nM (**Figure 6b, 6c**). Importantly, BPRPT245 not only increased intracellular 15-keto-PGE_2 concentrations in a dose-dependent manner (**Figure 6d**), but also

augmented insulin-stimulated glucose uptake of induced 3T3-L1 adipocytes (**Figure 6e**). Molecular docking showed that BPRPT245 interferes with the interaction between 15-keto-PGE_2 and NADPH within catalytic site of the PTGR2 (**Figure 6f**).

Our previous crystallographic study demonstrated that NADPH binding to PTGR2 was critical for subsequent binding of 15-keto-PGE_2 (25). NAPDH mainly binds with Tyr259 of PTGR2 through hydrogen bond (25), which was interfered by BPRPT245. BPRPT245 forms strong hydrogen bounding network with Tyr259, Arg53, and Cys54 of PTGR2; Pi-Pi sandwich with Tyr51 and Phe99 of PTGR2; and CH-Pi interaction with the nicotinamide ring of NADPH, resulting in disruption of the interaction between 15-keto-PGE_2, PTGR2 and NADPH (**Figure 6g**). Lineweaver–Burk plot further showed that BPRPT245 (50nM) is a competitive PTGR2 inhibitor (**Figure 6h**). The addition of BPRPT245 (50nM) change the Km between 15-keto-PGE_2 and PTGR2 from 29.06±0.77 to 64.04±12.34 (μM) (P=0.02) but Vmax remained unchanged, consistent with a competitive inhibitor model (**Figure 6i**).

We further examine the effect of BPRPT245 on obesity and insulin-resistance in mice by oral administration of BPRPT245 (100 mg/kg/day) in HFHSD-fed obese C57BL6/J mice. BPRPT245 significantly prevented diet-induced obesity (**Figure 6j**), lower fasting plasma glucose (**Figure 6k**), improved glucose tolerance (**Figure 6l**), and insulin sensitivity (**Figure 6m**) in mice. In addition, white fat mass and liver mass were significantly reduced by BPRPT245 treatment (**Figure 6n**). The extent of hepatic steatosis (**Figure 6o)** and hepatic triglycerides content were also significantly reduced **(Figure 6p**). F4/80 immunohistochemical stain of the perigonadal fat showed less F4/80-positive macrophages in mice receiving BPRPT245 than vehicle (**Figure 6q, 6r**). The adipocyte size was reduced in mice receiving BPRPT245 compared to vehicle (**Figure 6s**) but the adipocyte number was not changed (**Figure 6t**). Body composition analysis showed that BPRPT245 did not cause fluid retention (**Figure 6u**) and there is no difference of bone mineral density after BPRPT245 treatment for 26 weeks (**Figure 6v, 6w).** A summary graph depicted that increasing 15-keto-PGE_2 via inhibiting PTGR2 prevents diet-induced obesity, insulin resistance, glucose intolerance, and fatty liver without fluid retention and altered bone mineral density (**Figure 6x**).

Pharmacokinetic studies including the half-life, clearance, steady-state volume of distribution, maximum serum concentration, and oral bioavailability after single intravenous injection and oral gavage of BPRPT245 were shown in **Supplementary Table 4.** There was a trend of increased 15-keto-PGE_2 content in perigonadal fat (~1.34-fold increase) and significantly increased 15-keto-PGE_2 content in inguinal fat (~1.32-fold increase) of mice receiving BPRPT245 as compared to vehicle (**Supplementary Figure 10)**. The fat tissue concentration of BPRPT245 was shown in **Supplementary Figure 11.** Pathological examination of bone marrow, brain, heart, lung, kidney, pancreas, brown fat, and perigonadal fat of mice showed no significant difference between mice receiving BPRPT245 and vehicle for 26 weeks (**Supplementary Table 5**) and there was no differences in serum alanine aminotransferase (ALT), total bilirubin, blood urea nitrogen (BUN), and creatinine levels (**Supplementary Figure 12)**.

Discussion

In this study, we found that serum levels of endogenous PPARγ ligand 15-keto-PGE_2 is markedly reduced in obese mice and human subjects with type 2 diabetes. Increasing 15-keto-PGE_2 through either genetic disruption or chemical inhibition of its degrading enzyme PTGR2 or direct injection of 15-keto-PGE_2 to mice significantly improved insulin sensitivity and prevented diet-induced obesity. The insulin-sensitizing effect of 15-keto-PGE_2 is mediated through activating PPARγ by binding mode different from pioglitazone. These beneficial effects were devoid of side effects of pioglitazone, including weight gain, fluid retention and osteoporosis. Based on the hit compounds from high-throughput screening, we developed a PTGR2 small-molecule inhibitor that effectively prevented diet-induced obesity, improved insulin sensitivity and insulin tolerance without side effect of thiazolidinediones through increasing 15-keto-PGE_2 and PPARγ activation.

Several candidate endogenous PPARγ ligands have been proposed, including oxidized polyunsaturated fatty acids, nitrated fatty acids, eicosanoids, and serotonin metabolites (26-28). For example, 9-HODE (9-hydroxyoctadecadienoic acid) and 13-HODE (13-hydroxyoctadecadienoic acid), the oxidized linoleic acid metabolites, were found to be abundant in atherosclerotic plaques to induce CD36 expression on macrophages to uptake lipid through activation of PPARγ (29). 15-HETE (15-hydroxyeicosatetraenoic acid), a metabolite of arachidonic acid, was shown to promote adipocyte differentiation via PPARγ (30). Similarly, 15-deoxy-$\triangle^{12,14}$-PGJ_2 also induced adipocyte differentiation through PPARγ (31). Nitrated linoleic acid and oleic acid are potent PPARγ ligands that induce adipocyte differentiation (32). The metabolite of serotonin, 5-methyl-indole-acetate has been proposed as an endogenous PPARγ ligand that stimulates adipogenesis (33).

However, the identification of endogenous PPARγ ligands remains difficult. Their binding affinity, binding site, specific mode of action, and physiological concentrations remain to be defined. Previous structural analyses demonstrated that endogenous PPARγ ligands with an α, β-unsaturated moiety can form covalent bond with the human Cys285 (or murine Cys313) residue at helix 3 of PPARγ with a more stable thermal stability than other ligands (11,12, 34) and may thus serve as effective and physiologically relevant ligands. Our study confirmed that 15-keto-PGE_2 forms covalent binding with the cysteine 285 residue at helix 3 of PPARγ. Given the relative low concentrations of various proposed endogenous PPARγ ligands, the higher affinity of 15-keto-PGE_2 to PPARγ through covalent binding suggests that 15-keto-PGE_2 might be a physiologically functional PPARγ ligand. In support of the present findings, a recent systemic screen of 94 lipids by LC-MS/MS confirmed 15-keto-PGE_2 as an endogenous PPARγ ligand *in vivo* (13, 35).

The PPARγ LBD consists of 13 α-helices (helices 1-12) and four small β-sheets (β1-4) (36,37). The C-terminal AF-2 coactivator binding surface critical for recruitment of transcriptional co-activators contains helices 12, 3, 5, and 11, with helix 12 oriented outward. Helix 12 is highly mobile and the binding of classical full PPARγ agonists such as pioglitazone stabilizes helix 12. The stabilization of helix 12

recruits transcriptional co-activators such as SRC1 (steroid receptor coactivator 1) (38). However, several synthetic partial or selective PPARγ ligands including MRL-24 and SR1664, which exert potent anti-diabetic activity without causing fluid retention, weight gain, and osteoporosis, bind PPARγ within the pocket between helix 3 and β-sheets and preferentially stabilize β-sheets but not helix 12 (36-38) (**Supplementary Figure 8**). This conformational change may recruit other transcriptional coactivators such as TRAP220. This alternative binding mode is a helix 12-independent agonism for PPARγ (8, 39-42).

Here we demonstrate that 15-keto-PGE_2 improves insulin sensitivity via activation of PPARγ without the side effects of thiazolidinediones. The reasons for the absence of the side effects remain elusive but might be related to the alternative ligand-binding site of 15-keto-PGE_2. Full synthetic ligand pioglitazone preferentially stabilizes helix 12. In contrast, our docking modeling showed 15-keto-PGE_2 forms a covalent bond with helix 3, which restrains its binding pocket within helices 3, 5, and 7 and the β sheets, which is distant from helix 12 (**Figure 4c,d**). This binding pattern resembles the helix 12-independent agonism of MRL-24 and SR1664, which may explain the absence of the side effect of thiazolidinediones.

We found that either inhibition of PTGR2 or direct administration of 15-keto-PGE_2 increased fat browning and thermogenesis with increased *Ucp1* expression. We further demonstrated that this effect is adipocyte-autonomous. This finding is compatible with previous reports (43, 44) showing that chronic activation of PPARγ leads to fat browning and increased *Ucp1* expression. The increased *Ucp1* expression was previously thought to be mediated through binding to an enhancer upstream of the *Ucp1* gene or through stabilization of PRDM16 protein (44-46).

In addition, we screened a chemical library and further developed a small-molecule PTGR2 enzymatic inhibitor BPRTP245 that effectively increased intracellular 15-keto-PGE_2 levels, activated PPARγ, and promoted glucose uptake in adipocytes. Importantly, BPRTP245 prevented diet-induced obesity, improved insulin sensitivity, and reduced insulin intolerance without fluid retention and altered bone mineral density. Of note, a recent global mapping for lipid-interacting proteins also identified PTGR2 (47). Another global mapping for small-molecule fragment-protein interaction identified a fragment and its structural analogs that could inhibit PTGR2 enzymatic activity. These analogs inhibited PTGR2 activity and increased 15-keto-PGE_2-dependent PPARγ transcriptional activity *in vitro* (48), further supporting our concept that inhibition of PTGR2 effectively activates PPARγ. PTGR3 is a homologous protein of PTGR2 that shares 23% amino acid sequence homology with PTGR2. 15-keto-PGE_2 has been reported as a substrate of PTGR3 and knockdown of *Ptgr3* in adipocytes have been shown to activate PPARγ (24). We found that *Ptgr3* knockout mice markedly improve insulin sensitivity and glucose intolerance without side effects of thiazolidinediones (unpublished data). Taken together, these data strongly support the notion that increasing 15-keto-PGE_2 via inhibition of its degrading enzymes PTGR2 is an effective way to activate PPARγ without side effects of thiazolidinediones.

In conclusion, endogenous PPARγ ligand 15-keto-PGE_2 levels were reduced in diet-induced obese mice or in patients with type 2 diabetes. Serum 15-keto-PGE_2 is inversely associated with insulin resistance in

non-diabetic humans. Increasing the level of 15-keto-PGE_2 lead to improved insulin sensitivity and glucose tolerance, and protected against diet-induced obesity and fatty liver without side effects of thiazolidinediones. Therefore, the development of PTGR2 inhibitors to increase endogenous PPARγ ligand may be novel approach to treat type 2 diabetes.

Declarations

Acknowledgements

We thank the Gene Knockout Mice Core of the Medical College of National Taiwan University for generation of *Ptgr2* knockout mice. LTQ-Orbitrap data and additional technical assistance were performed by the Metabolomics Core Facility in the Scientific Instrument Center. The ultrahigh performance liquid chromatography and the ion trap-orbitrap mass spectrometer for quantification were supported by the Metabolomics Core Laboratory of the Agricultural Biotechnology Research Center at Academia Sinica in Taiwan. We thank the Taiwan Animal Consortium (MOST 107-2319-B-001-002) and the Taiwan Mouse Clinic for technical support in indirect calorimetry, body composition, tissue fixation and slide sectioning, bone mineral density, and H&E stain experiment. We thank the Department of Nuclear Medicine of National Taiwan University Hospital for small animal PET CT. The CRISPR/Cas9 and lentiviral system was provided by the RNA Technique and Gene Manipulation Core at the Genome Research Center of Academia Sinica. The drug screening was conducted by the ultra-high throughput screening (uHTS) core service of the Genome Research Center of Academia Sinica. We also thank the pathological core service of the National Laboratory Animal Center. This study was supported by MOST of Taiwan (104-2314-B-002-219-MY3, 106-2314-B-002-137-MY3, 106-2321-B-002-040, 107-2321-B-002-067) and National Taiwan University and National Taiwan University Hospital (UN105-0072, UN109-008).

Competing interests

All authors declared no conflict of interest

Data availability

The data that support the findings of this study are available from the authors on reasonable request, see author contributions for specific data sets.

Author contributions

Y.C.C., M.L.H. designed, conducted the experiments, and wrote the manuscript. L.K.T. conducted chemical synthesis (BPRPT245). S.Y.C. conducted cell-based experiments. Y.Y.K. conducted molecular docking. M.S.H. conducted pharmacokinetic experiments. S.W.H. conducted Immunoprecipitation. H.L.L. conducted proteomic analysis. F.H.H. generated cysteine-coupled 15-keto-PGE_2 and 15-keto-PGF_2 proteins. J.Y.N., J.Y.H., F.C.K. conducted animal experiments. W.S.Y., C.H.C. conducted the experiments. S.Y.L. generated knockout mouse. Y.R.C., Y.W.C., B.Y.L. conducted LC-MS/MS experiments. C.M.T., C.N.H., J.J.H. provided human serum samples. F.A.L. conducted proteomic experiments. J.C., Y.S. provided liposome. T.K.Y. conducted pharmacodynamic experiments. T.J.R.C. conducted high throughput drug screening. T.Y.C. conducted animal pathology experiments. Y.H.T., L.M.C. supervised the work, designed the experiments, and wrote the manuscript.

References

1. Ahmadian, M., Suh, J.M., Hah, N., Liddle, C., Atkins, A.R., Downes, M., Evans, R.M. PPARγ signaling and metabolism: the good, the bad and the future. *Nat. Med.* **19**, 557–566 (2013)
2. Soccio, R.E., Chen, E.R., Lazar, M.A. Thiazolidinediones and the promise of insulin sensitization in type 2 diabetes. *Cell Metab.* **20**, 573-91 (2014)
3. Wiviott, S.D., Raz, I., Bonaca, M.P., Mosenzon, O., Kato, E.T., Cahn, A., Silverman, M.G., Zelniker, T.A., Kuder, J.F., Murphy, S.A., Bhatt, D.L., Leiter, L.A., McGuire, D.K., Wilding, J.P.H., Ruff, C.T., Gause-Nilsson, I.A.M., Fredriksson, M., Johansson, P.A., Langkilde, A.M., Sabatine, M.S.; DECLARE–TIMI 58 Investigators. Dapagliflozin and Cardiovascular Outcomes in Type 2 Diabetes. *Engl. J. Med.* ***380,*** 347–357 (2019).
4. Marso, S.P., Daniels, G.H., Brown-Frandsen, K., Kristensen, P., Mann, J.F., Nauck, M.A., Nissen, S.E., Pocock, S., Poulter, N.R., Ravn, L.S., Steinberg, W.M., Stockner, M., Zinman, B., Bergenstal, R.M., Buse, J.B.; LEADER Steering Committee; LEADER Trial Investigators. Liraglutide and Cardiovascular Outcomes in Type 2 Diabetes. *Engl. J. Med.* **375**, 311-22 (2016)
5. DePaoli, A.M., Higgins, L.S., Henry, R.R., Mantzoros, C., Dunn, F.L.; INT131-007 Study Group. Can a selective PPARγ modulator improve glycemic control in patients with type 2 diabetes with fewer side effects compared with pioglitazone? *Diabetes Care.* **37**,1918-23 (2014)
6. Choi, J.H., Banks, A.S., Kamenecka, T.M., Busby, S.A., Chalmers, M.J., Kumar, N., Kuruvilla, D.S., Shin, Y., He, Y., Bruning, J.B., Marciano, D.P., Cameron, M.D., Laznik, D., Jurczak, M.J., Schürer, S.C., Vidović, D., Shulman, G.I., Spiegelman, B.M., Griffin, P.R. Antidiabetic actions of a non-agonist PPARγ ligand blocking Cdk5-mediated phosphorylation. **477**, 477-81(2011)
7. Choi, J.H., Banks, A.S., Estall, J.L., Kajimura, S., Boström, P., Laznik, D., Ruas, J.L., Chalmers, M.J., Kamenecka, T.M., Blüher, M., Griffin, PR., Spiegelman, B.M. Anti-diabetic drugs inhibit obesity-linked phosphorylation of PPARgamma by Cdk5. **466**, 451-6 (2010)
8. Bruning, J.B., Chalmers, M.J., Prasad, S., Busby, S.A., Kamenecka, T.M., He, Y., Nettles, K.W., Griffin, P.R. Partial agonists activate PPARgamma using a helix 12 independent mechanism. **15**, 1258-71

(2007)

9. Waki, H., Park, K.W., Mitro, N., Pei, L., Damoiseaux, R., Wilpitz, D.C., Reue, K., Saez, E., Tontonoz, P. The small molecule harmine is an antidiabetic cell-type-specific regulator of PPARgamma expression. *Cell Metab.* **5**, 357-70 (2007)
10. Chou, W.L., Chuang, L.M., Chou, C.C., Wang, A.H., Lawson, J.A., FitzGerald, G.A., Chang, Z.F. Identification of a novel prostaglandin reductase reveals the involvement of prostaglandin E2 catabolism in regulation of peroxisome proliferator-activated receptor gamma activation. *J Biol Chem*. **282**, 18162-72 (2007)
11. Waku, T., Shiraki, T., Oyama, T., Fujimoto, Y., Maebara, K., Kamiya, N., Jingami, H., Morikawa, K. Structural insight into PPARgamma activation through covalent modification with endogenous fatty acids. *J Mol Biol*. **385**, 188-99 (2009)
12. Shiraki, T., Kamiya, N., Shiki, S., Kodama, T.S., Kakizuka, A., Jingami, H. Alpha,beta-unsaturated ketone is a core moiety of natural ligands for covalent binding to peroxisome proliferator-activated receptor gamma. *J Biol Chem*. **280**,14145-53 (2005)
13. Harmon, G.S., Dumlao, D.S., Ng, D.T., Barrett, K.E., Dennis, E.A., Dong, H., Glass, C.K. Pharmacological correction of a defect in PPAR-gamma signaling ameliorates disease severity in Cftr-deficient mice. *Nat Med.* **16**, 313-8 (2010)
14. Chen, I.J., Hee, S.W., Liao, C.H., Lin, S.Y., Su, L., Shun, C.T., Chuang, L.M. Targeting the 15-keto-PGE2-PTGR2 axis modulates systemic inflammation and survival in experimental sepsis. *Free Radic Biol Med*. **115**, 113-126 (2018)
15. Cheng, C., Nakamura, A., Minamimoto, R., Shinoda, K., Tateishi, U., Goto, A., Kadowaki, T., Terauchi, Y., Inoue, T. Evaluation of organ-specific glucose metabolism by ¹⁸F-FDG in insulin receptor substrate-1 (IRS-1) knockout mice as a model of insulin resistance. *Ann Nucl Med*. **25**, 755-61 (2011)
16. Momcilovic, M., Bailey, S.T., Lee, J.T., Zamilpa, C., Jones, A., Abdelhady, G., Mansfield, J., Francis, K.P., Shackelford, D.B. Utilizing 18F-FDG PET/CT Imaging and Quantitative Histology to Measure Dynamic Changes in the Glucose Metabolism in Mouse Models of Lung Cancer. *J Vis Exp.* 57167 (2018)
17. Loening, A.M., Gambhir, S.S. AMIDE: a free software tool for multimodality medical image analysis. *Mol Imaging*. **2**, 131-7 (2003)
18. Ouyang, X., Zhou, S., Su, C.T., Ge, Z., Li, R., Kwoh, C.K. CovalentDock: automated covalent docking with parameterized covalent linkage energy estimation and molecular geometry constraints. *J Comput Chem*. **34**, 326-36 (2013)
19. Lee, M.A., Tan, L., Yang, H., Im, Y.G., Im, Y.J. Structures of PPARγ complexed with lobeglitazone and pioglitazone reveal key determinants for the recognition of antidiabetic drugs. *Sci Rep.* **7**, 16837 (2017)
20. Rigsby, R.E., Parker, A.B. Using the PyMOL application to reinforce visual understanding of protein structure. *Biochem Mol Biol Educ*. **44**, 433-7 (2016)

21. Dallakyan, S., Olson, A.J. Small-molecule library screening by docking with PyRx. *Methods Mol Biol.* **1263**, 243-50 (2015)
22. Laskowski, R.A., Swindells, M.B. LigPlot+: multiple ligand-protein interaction diagrams for drug discovery. *J Chem Inf Model*. **51**, 2778-86 (2011)
23. Chhajed, S.S., Shinde, P.E., Kshirsagar, S.J., Sangshetti, J.N., Gupta, P.P., Parab, M.M., Dasgupta, D. De-novo design and synthesis of conformationally restricted thiazolidine-2,4-dione analogues: highly selective PPAR-γ agonist in search of anti-diabetic agent. *Struct Chem* **31**, 1375–1385 (2020)
24. Yu, Y.H., Chang, Y.C., Su, T.H., Nong, J.Y., Li, C.C., Chuang, L.M. Prostaglandin reductase-3 negatively modulates adipogenesis through regulation of PPARγ activity. *J Lipid Res.* **54**, 2391-9 (2013)
25. Wu, Y.H., Ko, T.P., Guo, R.T., Hu, S.M., Chuang, L.M., Wang, A.H. Structural basis for catalytic and inhibitory mechanisms of human prostaglandin reductase PTGR2 *Structure.* **16**, 1714-23 (2008)
26. Krey, G., Braissant, O., L'Horset, F., Kalkhoven, E., Perroud, M., Parker, M.G., Wahli, W. Fatty acids, eicosanoids, and hypolipidemic agents identified as ligands of peroxisome proliferator-activated receptors by coactivator-dependent receptor ligand assay. *Mol Endocrinol.* **11**, 779-91(1997)
27. Kliewer, S.A., Sundseth, S.S., Jones, S.A., Brown, P.J., Wisely, G.B., Koble, C.S., Devchand, P., Wahli, W., Willson, T.M., Lenhard, J.M., Lehmann, J.M. Fatty acids and eicosanoids regulate gene expression through direct interactions with peroxisome proliferator-activated receptors alpha and gamma. *Proc Natl Acad Sci U S A.* **94**, 4318-23 (1997)
28. Forman, B.M., Tontonoz, P., Chen, J., Brun, R.P., Spiegelman, B.M., Evans, R.M. 15-Deoxy-delta 12, 14-prostaglandin J2 is a ligand for the adipocyte determination factor PPAR gamma. *Cell.* **83**, 803-12 (1995)
29. Nagy, L., Tontonoz, P., Alvarez, J.G., Chen, H., Evans, R.M. Oxidized LDL regulates macrophage gene expression through ligand activation of PPARgamma. *Cell.* **93**, 229-40 (1998)
30. Song, Y.S., Lee, D,H., Yu, J.H., Oh, D.K., Hong, J.T., Yoon, D.Y. Promotion of adipogenesis by 15-(S)-hydroxyeicosatetraenoic acid. *Prostaglandins Other Lipid Mediat.* **123**, 1-8 (2016)
31. Forman, B.M., Tontonoz, P., Chen, J., Brun, R.P., Spiegelman, B.M., Evans, R.M. 15-Deoxy-delta 12, 14-prostaglandin J2 is a ligand for the adipocyte determination factor PPAR gamma. *Cell.* **83**, 803-12 (1995)
32. Schopfer, F.J., Lin, Y., Baker, P.R., Cui, T., Garcia-Barrio, M., Zhang, J., Chen, K., Chen, Y.E., Freeman, B.A. Nitrolinoleic acid: an endogenous peroxisome proliferator-activated receptor gamma ligand. *Proc Natl Acad Sci U S A.***102**, 2340-5 (2005)
33. Itoh, T., Fairall, L., Amin, K., Inaba, Y., Szanto, A., Balint, B.L., Nagy, L., Yamamoto, K., Schwabe, J.W. Structural basis for the activation of PPARgamma by oxidized fatty acids. *Nat Struct Mol Biol.* **15**, 924-31 (2008)
34. Waku, T., Shiraki, T., Oyama, T., Maebara, K., Nakamori, R., Morikawa, K. The nuclear receptor PPARγ individually responds to serotonin- and fatty acid-metabolites. *EMBO J.* **29**, 3395-407 (2010)

35. Harmon, G.S., Lam, M.T., Glass, C.K. PPARs and lipid ligands in inflammation and metabolism. *Chem Rev.* **111**, 6321-40 (2011)
36. Nolte, R.T., Wisely, G.B., Westin, S., Cobb, J.E., Lambert, M.H., Kurokawa, R., Rosenfeld, M.G., Willson, T.M., Glass, C.K., Milburn, M.V. Ligand binding and co-activator assembly of the peroxisome proliferator-activated receptor-gamma. *Nature.* **395**, 137-43 (1998)
37. Zoete, V., Grosdidier, A., Michielin, O. Peroxisome proliferator-activated receptor structures: ligand specificity, molecular switch and interactions with regulators. *Biochim Biophys Acta.* **1771**, 915-25 (2007)
38. Chrisman, I.M., Nemetchek, M.D., de Vera, I.M.S., Shang, J., Heidari, Z., Long, Y., Reyes-Caballero, H., Galindo-Murillo, R., Cheatham, T.E. 3rd., Blayo. A.L., Shin. Y., Fuhrmann. J., Griffin. P.R., Kamenecka. T.M., Kojetin. D.J., Hughes, T.S. Defining a conformational ensemble that directs activation of PPARγ. *Nat Commun.* **9**, 1794 (2018)
39. Thangavel, N., Al Bratty, M., Akhtar Javed, S., Ahsan, W., Alhazmi, H.A. Targeting Peroxisome Proliferator-Activated Receptors Using Thiazolidinediones: Strategy for Design of Novel Antidiabetic Drugs. *Int J Med Chem.* **2017**,1069718 (2017)
40. Capelli, D., Cerchia, C., Montanari, R., Loiodice, F., Tortorella, P., Laghezza, A., Cervoni, L., Pochetti, G., Lavecchia, A. Structural basis for PPAR partial or full activation revealed by a novel ligand binding mode. *Sci Rep.* **6**, 34792 (2016)
41. Hughes, T.S., Chalmers, M.J., Novick, S., Kuruvilla, D.S., Chang, M.R., Kamenecka, T.M., Rance, M., Johnson, B.A., Burris, T.P., Griffin, P.R., Kojetin, D.J. Ligand and receptor dynamics contribute to the mechanism of graded PPARγ agonism. *Structure.* **20**, 139-50 (2012)
42. Hughes, T.S., Giri, P.K., de Vera I.M., Marciano, D.P., Kuruvilla, D.S., Shin, Y., Blayo, A.L., Kamenecka, T.M., Burris, T.P., Griffin, P.R., Kojetin, D.J. An alternate binding site for PPARγ ligands. *Nat Commun.* **5**, 3571 (2014)
43. Petrovic, N., Walden, T.B., Shabalina, I.G., Timmons, J.A., Cannon, B., Nedergaard, J. Chronic peroxisome proliferator-activated receptor gamma (PPARgamma) activation of epididymally derived white adipocyte cultures reveals a population of thermogenically competent, UCP1-containing adipocytes molecularly distinct from classic brown adipocytes. *J Biol Chem.* **285**, 7153-64 (2010)
44. Ohno, H., Shinoda, K., Spiegelman, B.M., Kajimura, S. PPARγ agonists induce a white-to-brown fat conversion through stabilization of PRDM16 protein. *Cell Metab.* **15**, 395-404 (2012)
45. Kozak, U.C., Kopecky, J., Teisinger, J., Enerbäck, S., Boyer, B., Kozak, L.P. An upstream enhancer regulating brown-fat-specific expression of the mitochondrial uncoupling protein gene. *Mol Cell Biol.* 14, 59-67 (1994)
46. Cassard-Doulcier, A.M., Gelly, C., Fox, N., Schrementi, J., Raimbault, S., Klaus, S., Forest, C., Bouillaud, F., Ricquier, D. Tissue-specific and beta-adrenergic regulation of the mitochondrial uncoupling protein gene: control by cis-acting elements in the 5'-flanking region. *Mol Endocrinol.* **7**, 497-506 (1993)
47. Niphakis, M.J., Lum, K.M., Cognetta, A.B. 3rd., Correia, B.E., Ichu, T.A., Olucha, J., Brown, S.J., Kundu, S., Piscitelli, F., Rosen, H., Cravatt, B.F. A Global Map of Lipid-Binding Proteins and Their Ligandability

in Cells. *Cell.* **161**, 1668-80 (2015)

48. Parker, C.G., Galmozzi, A., Wang, Y., Correia, B.E., Sasaki, K., Joslyn, C.M., Kim, A.S., Cavallaro, C.L., Lawrence, R.M., Johnson, S.R., Narvaiza, I., Saez, E., Cravatt, B.F. Ligand and Target Discovery by Fragment-Based Screening in Human Cells. *Cell.* **168**, 527-541 (2017)

Figures

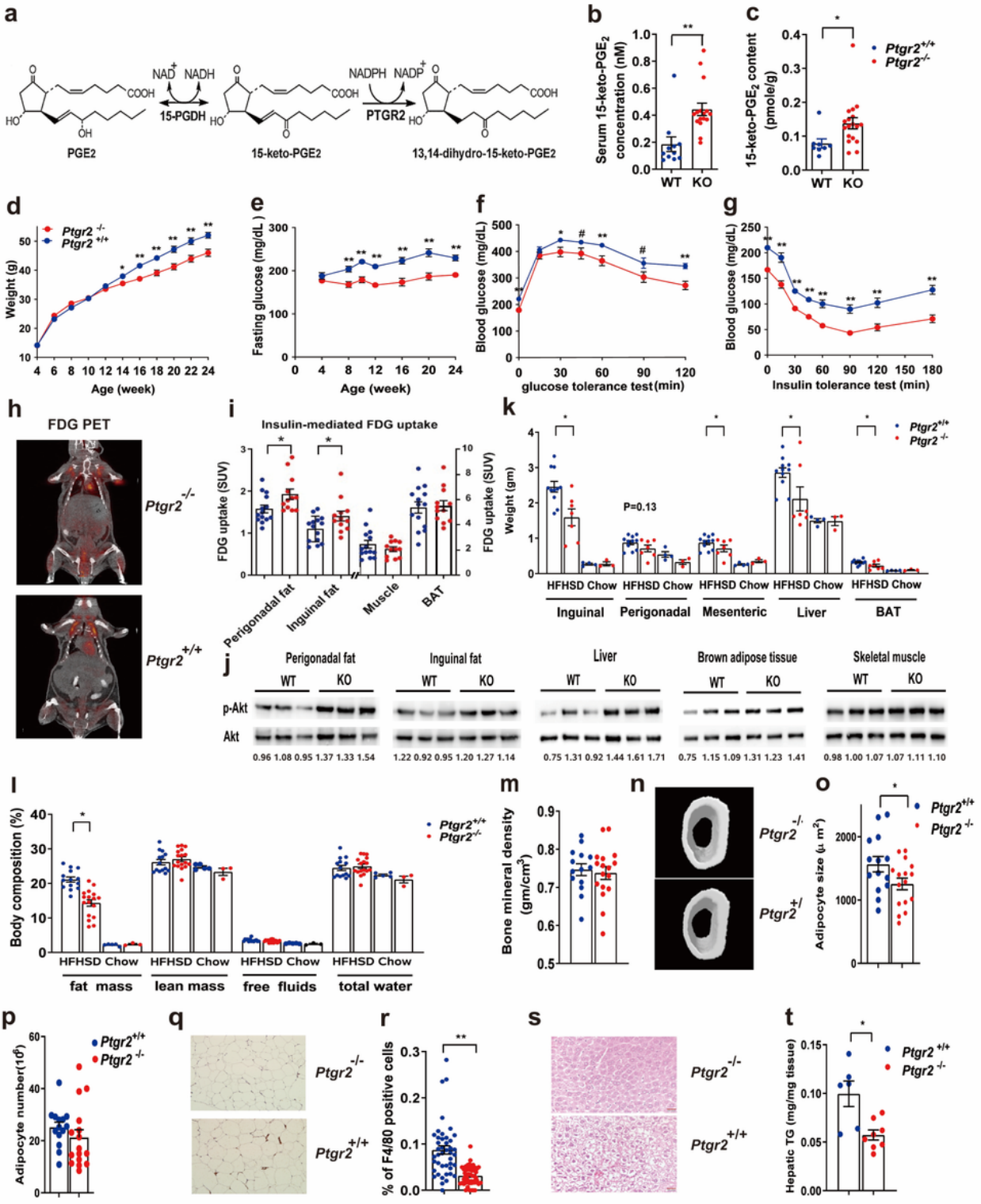

Figure 1

a Metabolism of 15-keto-PGE2. b Serum 15-keto-PGE2 levels (n=8:18). c 15-keto-PGE2 level in inguinal fat (n=11:16) measured by liquid chromatography (LC)-tandem mass spectrometry (MS/MS) (n=8:18) of Ptgr2 -/- mice and Ptgr2 +/+ on high-fat high-sucrose diet (HFHSD). d Body weight (n=20:21), e fasting glucose (n=20:21), and f glycemic level during intraperitoneal glucose tolerance test (ipGTT) (n=20:21) and g insulin tolerance test (ITT) (n=20:21) of Ptgr2 -/- and Ptgr2 +/+ mice on high-fat high-sucrose diet (HFHSD). h18F-FDG PET scan of Ptgr2 -/- and Ptgr2 +/+ mice after injection of glucose and insulin. i 18F-FDG uptake in perigonadal fat, inguinal fat, skeletal muscle, and brown adipose tissue after injection of glucose and insulin (n=14:12). j Phospho-Akt level after intraperitoneal insulin injection in perigonadal fat, inguinal fat, skeletal muscle, and brown adipose tissue. k Tissue weight of perigonadal fat, inguinal fat, mesenteric fat, liver, brown adipose tissue (n=11:7). l Body composition (n=14:17), m bone mineral density of femur(14:17), n micro computed tomography (CT) image of femur (n=14:17), o Average adipocyte size and p number n=(14:17). q F4/80 immunohistochemical stain of perigonadal fat. r Percentage of F4/80-positive cells in perigonadal fat(n=43:56). s H&E stain of liver and t hepatic triglyceride contents of (n=6:8) of Ptgr2 -/- mice and Ptgr2 +/+ on high-fat high-sucrose diet (HFHSD). * P < 0.05, **P< 0.01, ***P<0.001

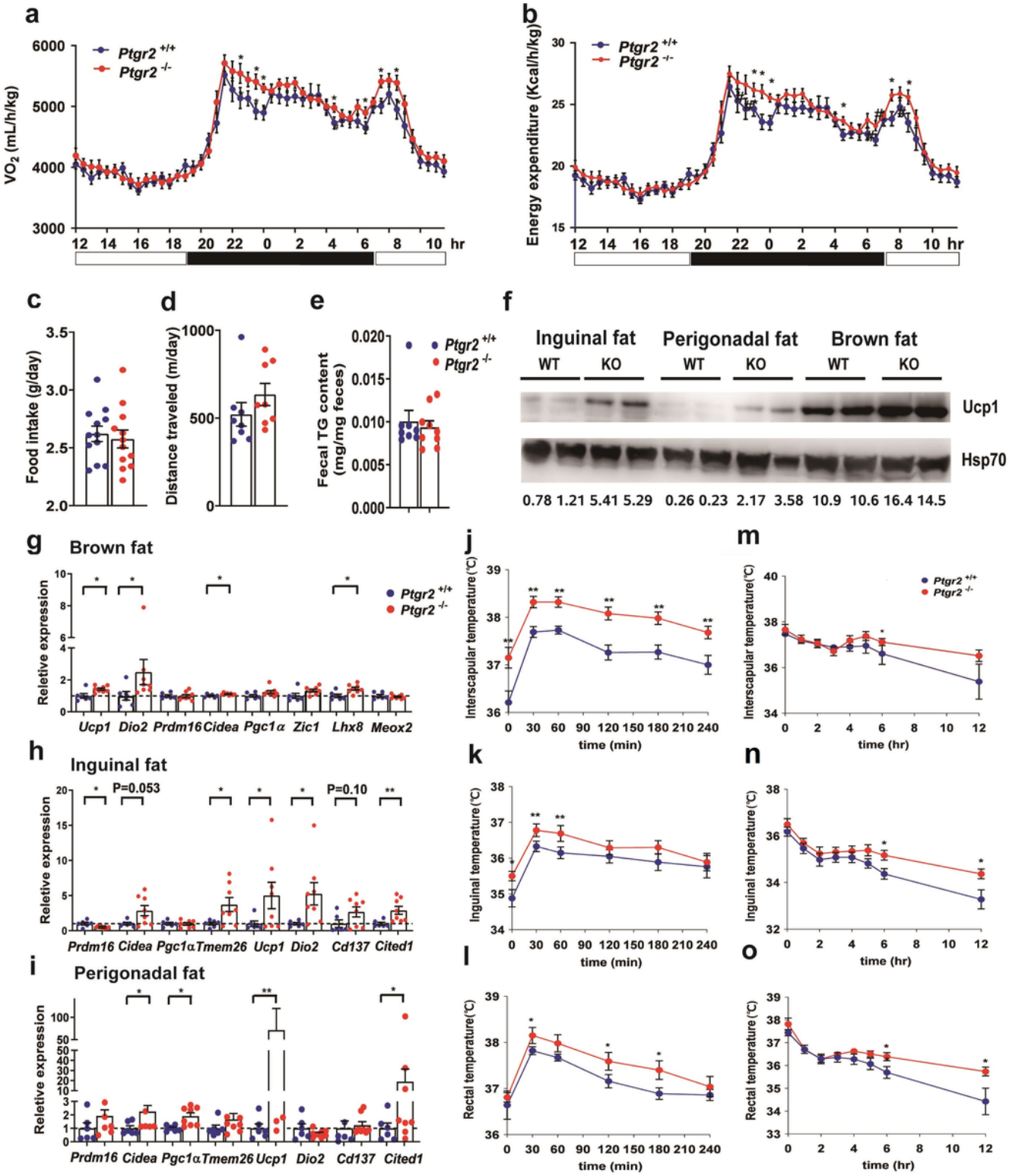

Figure 2

a O2 consumption (the white bar indicate the light-up time, the black bar indicate light-off time)(n=12:12) b energy expenditure (n=12:12), c food intake (n=12:12), d distance traveled (n=12:12), e fecal triglyceride content (n=8:9), f Immunoblots showing UCP1 level in different fat pads. g h, i, RT-qPCR of genes involved in browning of brown adipose tissue, inguinal fat and perigonadal fat (n=6:8). For the diet-induced thermogenesis test, 24-week-old mice were fasted overnight. Body surface including j interscapular area,

k inguinal area and l core rectal temperature at 0, 30, 60, 90, 120, 150, 180, and 240 min after HFHSD refeeding (n=14:16). For, cold tolerance test, mice were place in 4°C environments. Body surface temperature in m interscapular area, n inguinal area and o rectal temperature during cold tolerance test of Ptgr2 -/- mice and Ptgr2 +/+ mice on HFHSD (n=14:16). * P < 0.05 **P< 0.01, ***P<0.001

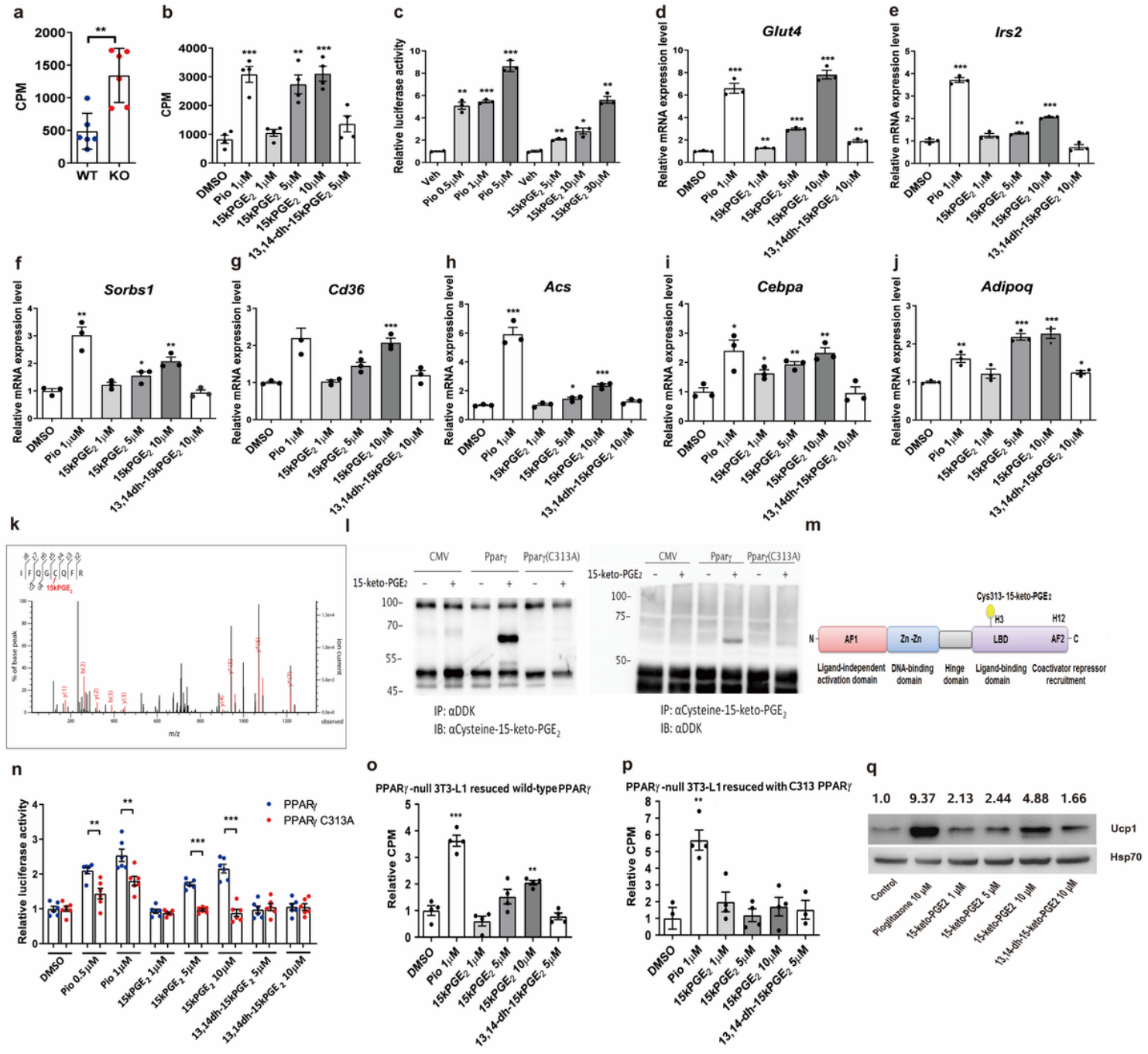

Figure 3

a Insulin-stimulated glucose uptake in primary white adipocytes isolated from Ptgr2 -/- and Ptgr2 +/+ mice. Insulin-mediated glucose uptake was shown by subtracting insulin-stimulated glucose uptake with basal glucose uptake (n=6:6). b Effect of 15-keto-PGE2 on insulin-stimulated glucose uptake in induced 3T3-L1 adipocytes (n=4 per grpup). c Activation of PPARγ measured by Gal-PPARγ/UAS-LUC reporter

assay in HEK293T cells (n=3 per grop). Cells were transfected with Gal4-PPARγ, UASG, and TK-Rluc (Renilla luciferase), and treated with pioglitazone or 15-keto-PGE2. RT-qPCR of d Glut4 and other PPARγ-downstream genes including e Irs2, f Sorbs1, g Cd36, h Acs, i Cepba, and j Adipoq in induced 3T3-L1 adipocytes treated with 15-keto-PGE2 (n=3 per group). k HEK293T cells transfected by murine PPARγ and treated with 15-keto-PGE2. Covalent binding of 15-keto-PGE2 to PPARγ detected by liquid-chromatography tandem mass spectrometry (LC-MSMS). l Reciprocal co-immunoprecipitation of mPPARγ and Cys-15-keto-PGE2. Myc-DDK-mPPARγ and Myc-DDK-mPPARγ C313A were expressed in HEK293T cells, and immunoprecipitation (IP) conducted using either anti-DDK (anti-Flag) or anti-15-keto-PGE2-cysteine-BSA antibody, followed by immunoblotting with anti-15-keto-PGE2-cysteine-BSA and anti-DDK antibody. m Diagram showing the motifs of PPARγ and 15-keto-PGE2 binding site. n PPRE reporter activity after addition of 15-keto-PGE2 in HEK293T cells transfected with wild-type and C313A mutant mPPARγ. Effect of 15-keto-PGE2 on insulin-stimulated glucose uptake in PPARγ-null cell line #1296 rescued with (n=3:3) o wild-type and p C313A mutant PPARγ by lentiviral transduction (n=4 per group). q Effect of pioglitazone, 15-keto-PGE2, and 13,14-dihydro-15-keto-PGE2 on Ucp1 expression in induced 3T3-L1 adipocytes for 3 weeks (n=4 per group). * P < 0.05, **P< 0.01, ***P<0.001.

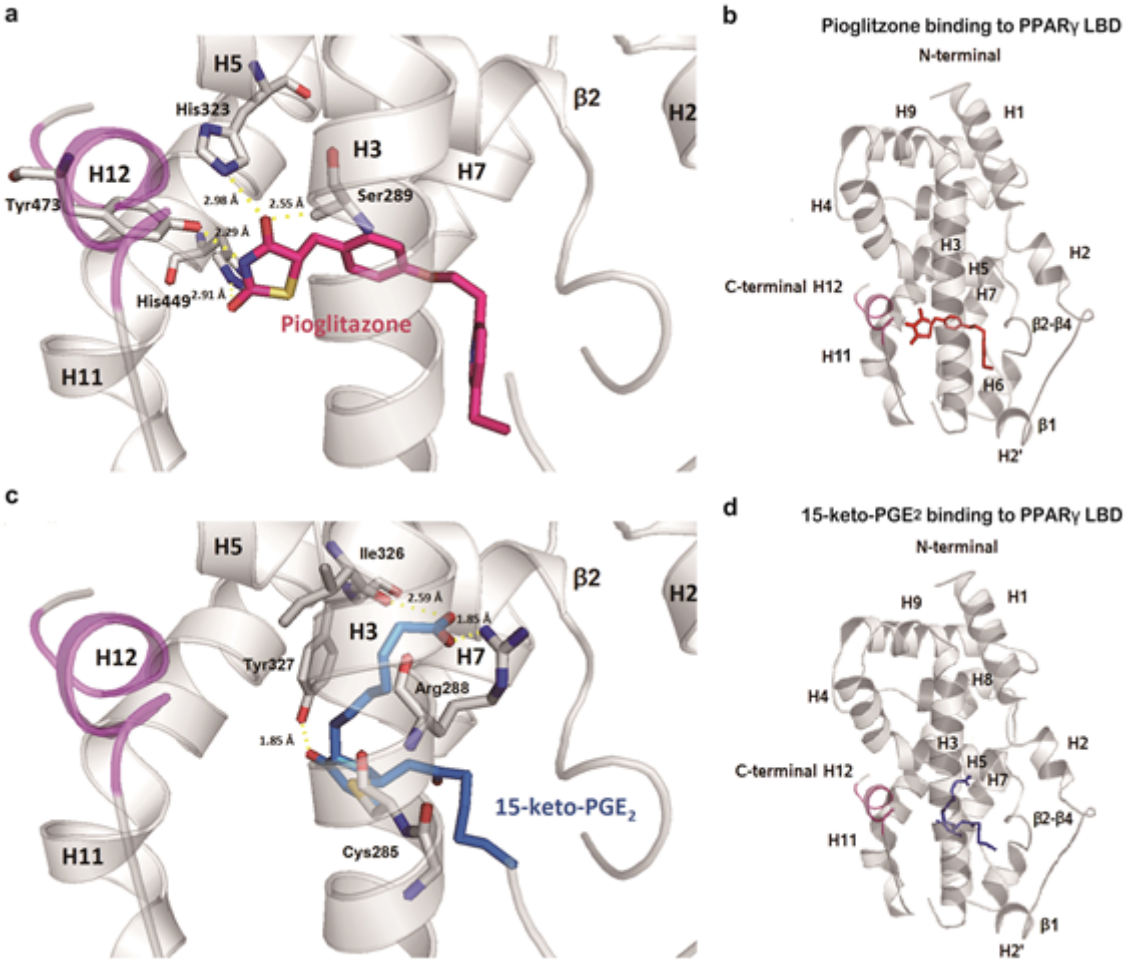

Figure 4

a The binding of pioglitazone (dark red) within human PPAR□ ligand-binding domain (LBD) determined from the X-ray co-crystal structure (PDB ID: 5Y2O). Pioglitazone forms a hydrogen bond with the Tyr473 (helix 12), Ser289 (helix 3), His323 (helix 5), and His449 (helix 11) residues. b Molecular docking showing the binding pocket of pioglitazone (dark red) within hPPARγ LBD. c The binding of 15-keto-PGE2 (blue) to the hPPAR□ LBD. 15-keto-PGE2 forms a covalent bond with the Cys285 (helix 3) residue and hydrogen bonds with Arg288 (helix 3), Ile326 (helix 5), and Tyr327 (helix 5) residues. d Molecular docking showing the binding pocket of 15-keto-PGE2 (blue) to hPPARγ LBD. C-terminal helix 12 is marked in purple.

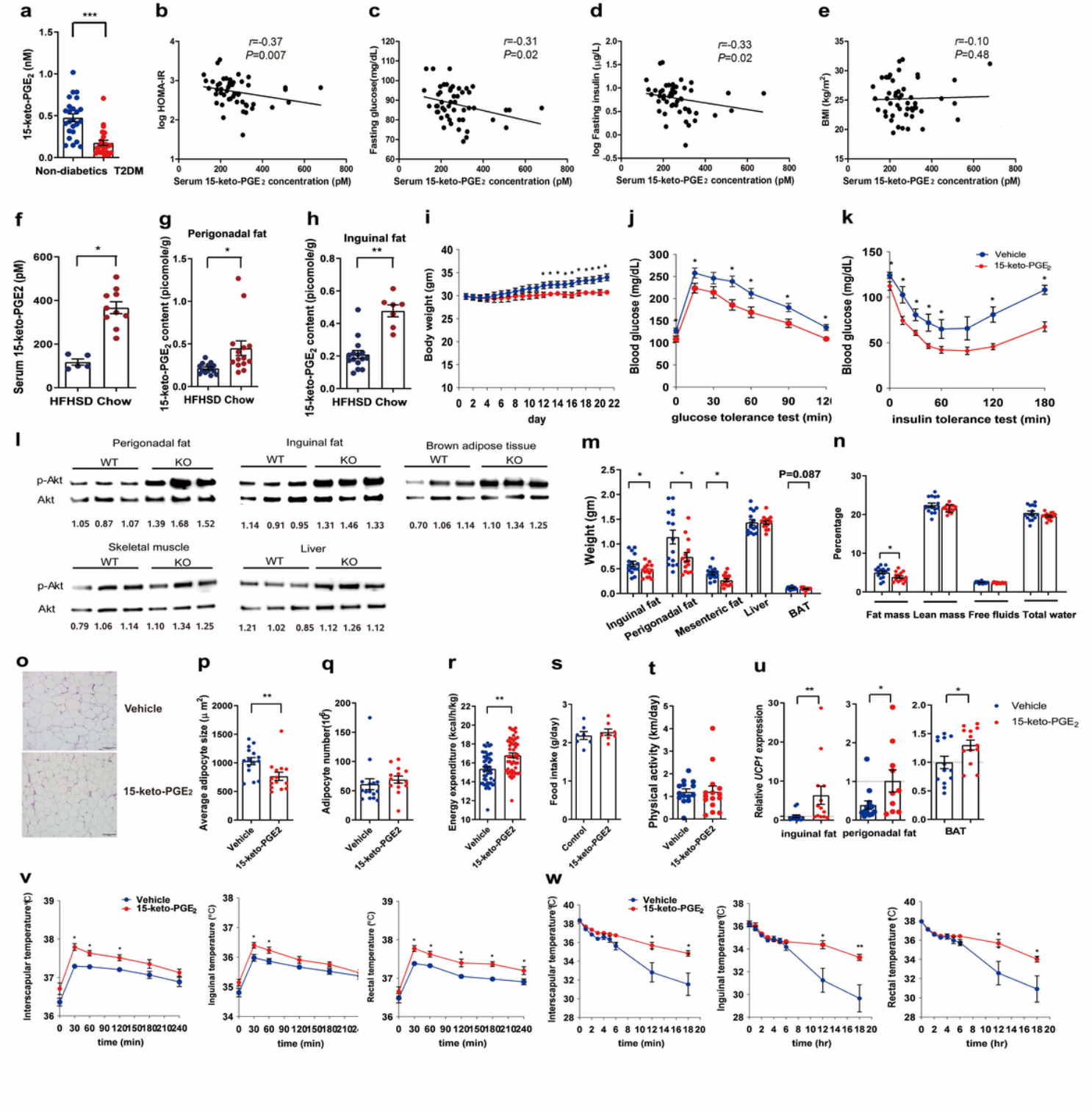

Figure 5

a Serum 15-keto-PGE2 concentration of non-diabetic human subjects and patients with type 2 diabetic patients. Correlation of serum 15-keto-PGE2 with (n=24:24) b log homeostasis model assessment of insulin resistance (log HOMA-IR), c fasting glucose, d, log fasting insulin e body mass index (BMI) in 50 non-diabetic human subjects. f Serum 15-keto-PGE2 concentration (n=5:10) and 15-keto-PGE2 content in g perigonadal fat (n=14:14) and h inguinal fat (n=15:7) of C57BL6/J mice on high-fat high-sucrose diet (HFHSD) or chow. i Body weight(n=15:15) and glucose levels during j intraperitoneal glucose tolerance test (ipGTT) (n=15:15)and k insulin tolerance test (ITT) (n=15:15) l Phospho-Akt levels in perigonadal fat, inguinal fat, muscle, and brown adipose tissue after intraperitoneal insulin injection. m Weight of perigonadal fat, inguinal fat, mesenteric fat, skeletal muscle, and brown adipose tissue of HFHSD-fed C57BL6/J mice treated with 15-keto-PGE2 and vehicle (n=15:15). u. Relative Ucp1 expression in inguinal fat, perigonadal fat, and brown adipose tissue of HFHSD-fed C57BL6/J mice treated with 15-keto-PGE2 and vehicle (n=13-14 per group). o H&E stain of perigonadal fat, p average adipocyte size, and q adipocyte number (n=15:15). r Energy expenditure measured by indirect calorimetry (n=15:15), s food intake (n=15:15), and t physical activity (n=15:15) of HFHSD-fed C57BL6/J mice treated with 15-keto-PGE2 and vehicle. n Body composition of HFHSD-fed C57BL6/J mice treated with 15-keto-PGE2 or vehicle (n=15:15) v. Body surface temperature of interscapular area, inguinal area, and rectal temperatures of 15-keto-PGE2-treated mice and vehicle control mice after HFHSD feeding (n=15:15). w. Body surface temperature of interscapular area, inguinal area, and rectal temperatures of 15-keto-PGE2-treated mice and vehicle control mice during cold test(n=15:15).* P < 0.05, **P< 0.01, ***P<0.001

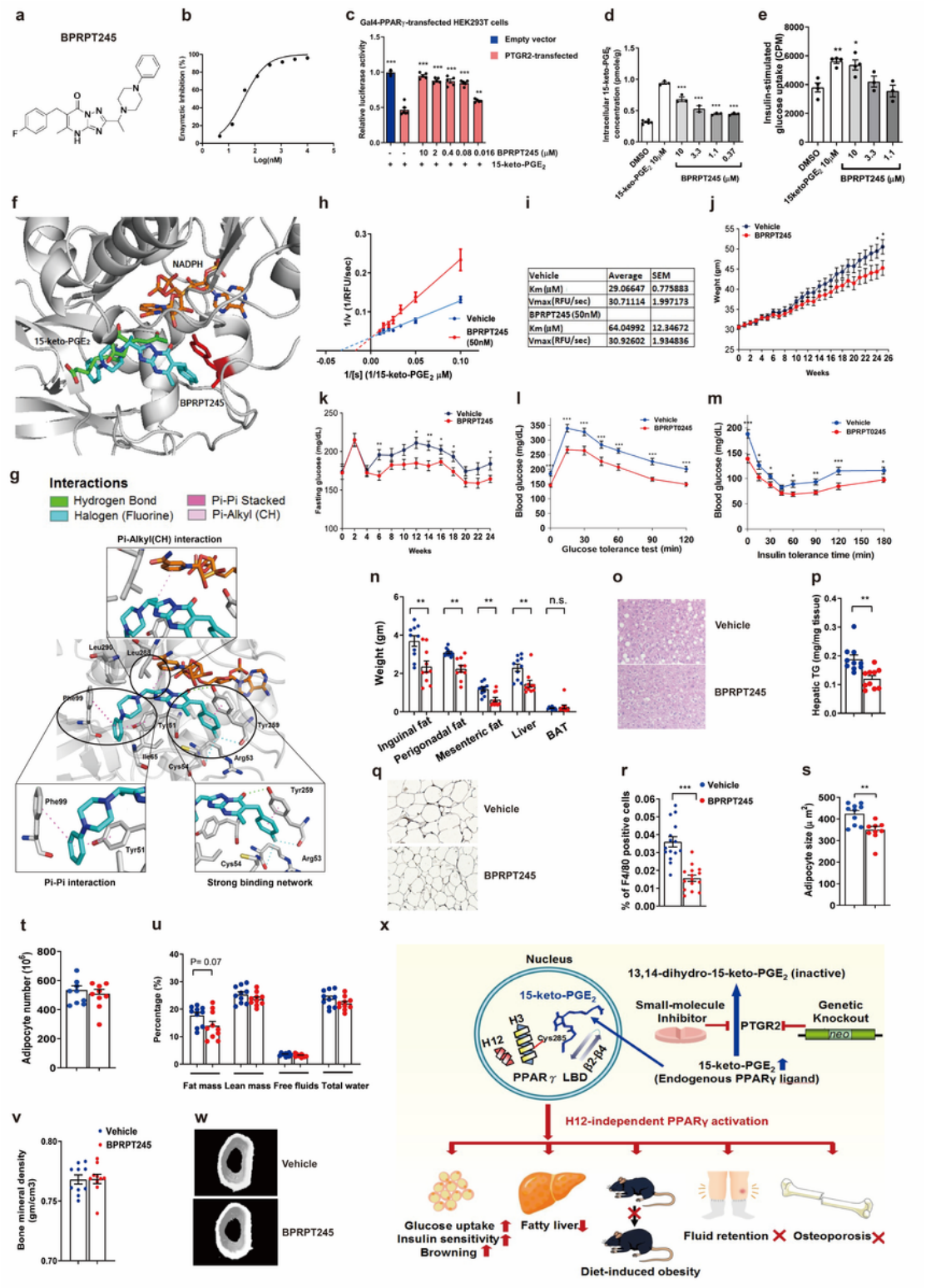

Figure 6

a Structure of BPRPT245. b Half-maximal inhibitory concentration (IC50) of BPRPT245. c Effect of BPRPT245 on 15-keto-PGE2-dependent PPARγ transcriptional activity in PTGR2-transfected HEK293T cells (n=5 per group). d Intracellular 15-keto-PGE2 content of induced 3T3-L1 adipocytes treated with BPRPT245 (n=3-6 per group) e Insulin-stimulated glucose uptake of induced 3T3-L1adipocytes treated with BPRPT245 (n=3-4 per group) f Molecular docking of 15-keto-PGE2 (green), NADPH (orange brown),

and BPRPT245 (cyan) of PTGR2,Tyr259 (red) of PTGR2. g Molecular docking showing that PTGR2 inhibitor BPRPT245 (cyan) interferes the interaction between 15-keto-PGE2 and NADPH through strong biding network, Pi-Alkyl(CH) interaction, and Pi-Pi interaction with PTGR2 and NADPH h Lineweaver–Burk plots showing the competitive inhibitory action of BPRPT245 (50 μM) for the interaction between 15-keto-PGE2 and PTGR2 (n=5) i values of Vmax and Km for 15-keto-PGE2 with or without the addition of BPRPT245 (50 μM) (n=5) j Body weight (n=15:15) k fasting glucose (n=15:15), l glycemic level during intraperitoneal glucose tolerance test (ipGTT) (n=15:15) and m insulin tolerance test (ITT (n=15:15), n tissue weight of perigonadal fat, inguinal fat, mesenteric fat, liver, brown adipose tissue (n=10:10), o representative H&E stain of liver section, p hepatic triglycerides content (n=10:10), q F4/80 immunohistochemical stain of gonadal fat, r percentage of F4/80-positive in perigonadal fat (n=15:15), s adipocyte size (n=10:10), t adipocyte number of perigonadal fat (n=10:10), u body composition (n=10:10), v bone mineral density (n=10:10), and w micro computed tomography (CT) image of femur of C57BL6/J mice ((n=10:10) x summary graph depicting that increasing 15-keto-PGE2 via inhibition of PTGR2 prevents diet-induced obesity, insulin resistance, glucose intolerance, and fatty liver without fluid retention and reduced bone mineral density. * P < 0.05, **P< 0.01, ***P<0.001

Supplementary Files

This is a list of supplementary files associated with this preprint. Click to download.

- SupplementaryMaterial.docx